Redox Modification of the Iron-Sulfur Glutaredoxin GRXS17 Activates Holdase Activity and Protects Plants from Heat Stress

Laura Martins, Johannes Knuesting, Laetitia Bariat, Avilien Dard, Sven Freibert, Christophe Marchand, David Young, Nguyen Ho Thuy Dung, Wilhelm Voth, Anne Debures, et al.

Plant Physiology Preview. Published on August 21, 2020, as DOI:10.1104/pp.20.00906

Short title: Redox-dependent chaperone of GRXS17

Redox modification of the Fe-S glutaredoxin GRXS17 activates holdase activity and protects plants from heat stress

Laura Martins[1,2,#], Johannes Knuesting[3,#], Laetitia Bariat[1,2], Avilien Dard[1,2], Sven A. Freibert[4], Christophe H. Marchand[5], David Young[6,7,8], Nguyen Ho Thuy Dung[6,7,8], Wilhelm Voth[9], Anne Debures[1,2], Julio Saez-Vasquez[1,2], Stéphane D. Lemaire[5,10], Roland Lill[4], Joris Messens[6,7,8], Renate Scheibe[3], Jean-Philippe Reichheld[1,2,*], Christophe Riondet[1,2]

[1] Laboratoire Génome et Développement des Plantes, Université Perpignan Via Domitia, F-66860 Perpignan, France;

[2] Laboratoire Génome et Développement des Plantes, CNRS, F-66860 Perpignan, France;

[3] Department of Plant Physiology, FB5, University of Osnabrück, D–49069 Osnabrueck, Germany;

[4] Institut für Zytobiologie und Zytopathologie, Philipps-Universität, Robert-Koch-Strasse 6, Marburg 35032, Germany;

[5] Institut de Biologie Physico-Chimique, UMR8226, CNRS, Sorbonne Université, F-75005 Paris, France;

[6] VIB-VUB Center for Structural Biology, 1050 Brussels, Belgium;

[7] Brussels Center for Redox Biology, 1050 Brussels, Belgium;

[8] Structural Biology Brussels, Vrije Universiteit Brussel, 1050 Brussels, Belgium;

[9] Department of Molecular, Cellular and Developmental Biology, University of Michigan, Ann Arbor, MI 48109, USA

[10] Institut de Biologie Paris-Seine, Laboratory of Computational and Quantitative Biology, UMR7238, CNRS, Sorbonne Université, F-75005 Paris, France;

[#] These authors contributed equally to this work.

* To whom correspondence should be addressed: E-mail: jpr@univ-perp.fr.

Jean-Philippe Reichheld, Tel: +33 4 68662225; Fax: +33 4 68668499; E-mail: jpr@univ-perp.fr.

Laboratoire Génome et Développement des Plantes, Université Perpignan Via Domitia, F-66860 Perpignan, France.

One-sentence summary

A cysteine-dependent redox modification of the iron-sulfur cluster glutaredoxin GRXS17 activates its holdase activity and protects plants from heat stress

AUTHOR CONTRIBUTION

LM, JK, JSV, SDL, RL, JM, RS, JPR and CR designed the research; LM, JK, LB, AD, SAF, CHM, DY, NHTD, and AD performed the research; SAF, CHM, DY, NHTD, SDL, RL and JM contributed new reagents/analytic tools; LM, JK, AD, SAF, CHM, DY, JSV, SDL, RL, JM, RS, JPR, and CR analyzed the data; and LM, JK, SAF, DY, JSV, SDL, RL, JM, RS, JPR and CR wrote the paper.

ABSTRACT

Heat stress induces misfolding and aggregation of proteins unless they are guarded by chaperone systems. Here, we examined the function of the glutaredoxin GRXS17, a member of thiol reductase families in the model plant Arabidopsis (*Arabidopsis thaliana*). GRXS17 is a nucleocytosolic monothiol glutaredoxin consisting of an N-terminal thioredoxin (TRX)-domain and three CGFS-active site motif-containing GRX-domains that coordinate three iron-sulfur (Fe-S) clusters in a glutathione (GSH)-dependent manner. As a Fe-S cluster-charged holoenzyme, GRXS17 is likely involved in the maturation of cytosolic and nuclear Fe-S proteins. In addition to its role in cluster biogenesis, GRXS17 presented both foldase and redox-dependent holdase activities. Oxidative stress in combination with heat stress induced loss of its Fe-S clusters followed by subsequent formation of disulfide bonds between conserved active site cysteines in the corresponding TRX domains. This oxidation led to a shift of GRXS17 to a high-molecular weight complex and thus activated its holdase activity *in vitro*. Moreover, GRXS17 was specifically involved in plant tolerance to moderate high temperature and protected root meristematic cells from heat-induced cell death. Finally, GRXS17 interacted with a different set of proteins upon heat stress, possibly protecting them from heat injuries. Therefore, we propose that the Fe-S cluster enzyme glutaredoxin GRXS17 is an essential guard that protects proteins against moderate heat stress, likely through a redox-dependent chaperone activity. We reveal the mechanism of an Fe-S cluster-dependent activity shift that converts the holoenzyme GRXS17 into a holdase, thereby preventing damage caused by heat stress.

INTRODUCTION

Glutaredoxins (GRX) are small ubiquitous thiol reductases belonging to the thioredoxin (TRX) superfamily (Rouhier et al., 2008; Meyer et al., 2009). Most living organisms harbour two GRX classes (I and II), whereas additional classes are found in specific genera, including plants (Couturier et al., 2009). GRX from class I exhibit oxidoreductase activities, controlling thiol redox homeostasis of many proteins mostly through glutathionylation/deglutathionylation activities. This activity generally depends on glutathione (GSH) as a reductant and relies on an active site harboring at least one cysteine (Meyer et al., 2012). GRX from class II are involved in the regulation of iron (Fe) metabolism and in the maturation of iron-sulfur (Fe-S) proteins (Mühlenhoff et al., 2010; Haunhorst et al., 2013; Couturier et al., 2013). This function relies on their capacity to bind a labile iron-sulfur cluster (Fe-S cluster) and to transfer it to other Fe-S-containing proteins (Zhang et al., 2011; Banci et al., 2015; Frey et al., 2016), and to interact with BolA proteins (reviewed by (Couturier et al., 2015; Rey et al., 2019). The Fe-S cluster in class II GRX is coordinated by a conserved monocysteinic active site (CGFS) and a glutathione molecule, a feature largely conserved within eukaryotic organisms (Lillig et al., 2005; Wingert et al., 2005; Rouhier et al., 2007; Bandyopadhyay et al., 2008; Couturier et al., 2011; Riondet et al., 2012; Berndt and Lillig, 2017).

In the model plant Arabidopsis (*Arabidopsis thaliana*), class II GRXs are called GRXS14 (At3g54900), GRXS15 (At3g15660), GRXS16 (At2g38270) and GRXS17 (At4g04950; Supplemental Figure 1). They share the capacity to bind and exchange Fe-S clusters with different client proteins, like ferredoxins and aconitase (Bandyopadhyay et al., 2008; Moseler et al., 2015). Consistent with this activity, most plant type-II GRX are able to rescue defects of the budding yeast (*Saccharomyces cerevisiae*) *grx5* mutant deficient in mitochondrial Fe-S cluster biogenesis, underlying their involvement in maturation of Fe-S proteins (Molina et al., 2004; Liu et al., 2013; Knuesting et al., 2015; Moseler et al., 2015). Nevertheless, evidence for their implication in the

biogenesis of Fe-S proteins are poorly described *in vivo*. Arabidopsis plants deficient for the plastidic GRXS14 exhibit accelerated chlorophyll loss upon prolonged darkness, leading to a decreased abundance of proteins acting in Fe-S cluster metabolism (Rey et al., 2017).

PICOT (PKC-interacting cousin of thioredoxin)-like GRX are multi-domain type-II GRX found in the cytosol of most eukaryotic organisms (Berndt and Lillig, 2017). In most organisms, PICOT proteins are composed of one or two adjacent GRX domains with a CGFS active-site sequence motif preceded by a TRX domain. The PICOT proteins of vascular plants, like GRXS17, contain a third CGFS-containing GRX domain (Supplemental Figure 1; Couturier et al., 2009). *In vitro*, GRXS17 is a homodimer and each GRX-CGFS domain coordinates an Fe-S cluster in a GSH-dependent manner (Knuesting et al., 2015). Similarly to other class II GRX, GRXS17 is capable of complementing the defect of the yeast *grx5* deletion mutant, likely by transferring Fe-S clusters to mitochondrial acceptor proteins (Bandyopadhyay et al., 2008; Knuesting et al., 2015). Affinity chromatography approaches with crude extracts have shown that GRXS17 associates with known cytosolic iron-sulfur protein assembly (CIA) components like METHIONINE REQUIRING18/METHYL METHANESULFONATE19 (MET18/MMS19), DEREPRESSED FOR RIBOSOMAL PROTEIN S14 EXPRESSION (DRE2), and with other cytosolic Fe-S cluster-containing proteins like XANTHINE DEHYDROGENASE1 (XDH1) and CYTOSOLIC THIOURIDYLASE SUBUNIT1 (CTU1) and CTU2 (Iñigo et al., 2016; Wang et al., 2019). However, Arabidopsis *grxs17* null mutants have only a minor decrease in cytosolic Fe-S enzyme activities, indicating that GRXS17 likely does not play a major role in *de novo* Fe-S cluster assembly in the cytosol (Knuesting et al., 2015). Genetic evidence from different plant species suggests a protective role of GRXS17 during thermal, genotoxic and drought stress (Cheng et al., 2011; Wu et al., 2012; Iñigo et al., 2016; Hu et al., 2017; Wu et al., 2017), in meristem development (Knuesting et al., 2015), hormonal responses (Cheng et al., 2011), and in integrating redox homeostasis and iron deficiency responses (Yu et al., 2017). Nevertheless, for most of these functions, the underlying mechanism and targets remain enigmatic.

GRXS17 interacts with BolA2 and other cytosolic or nuclear protein partners (i.e. NF-YC11) which do not contain Fe-S clusters, suggesting that GRXS17 may have other functions than its Fe-S cluster metabolism activity (i.e. oxidoreductase or chaperone activities; Couturier et al., 2014; Knuesting et al., 2015; Iñigo et al., 2016). Indeed, in their apo-form, other Fe-S-containing GRXs, like the human Grx2 and the plant GRXC1, function as thiol reductases and are proposed to act as redox sensors for the activation of antioxidant enzymes in oxidative stress conditions (Lillig et al., 2005; Rouhier et al., 2007; Zaffagnini et al., 2008; Couturier et al., 2011; Riondet et al., 2012). Moreover, thiol reductases from different types exhibit moonlighting functions like endonuclease (Liu et al., 2013) and chaperone activities (Lee et al., 2009; Park et al., 2009; Chae et al., 2013). Therefore, the labile character of the Fe-S cluster of GRX suggests that the holo- and apo-forms might perform different activities under stress conditions.

Here, we address this question by exploring GRXS17 properties under oxidative and heat stress conditions. We found that, when subjected to oxidative conditions, reconstituted holo-GRXS17 rapidly loses its Fe-S cluster and becomes a cysteine-dependent holdase. The switch to holdase involves oligomerization. Moreover, GRXS17 exhibited also a weak foldase activity which does not depend on its active-site cysteines. To confirm the *in vivo* importance of these chaperone activities of GRXS17, we analysed a *grxs17* knock-out mutant highly sensitive to heat stress. Mutant complementation experiments with several cysteine variants of GRXS17 indicated the crucial role of the active-site cysteines in protecting proteins during heat stress. Finally, GRXS17 associated with a different set of partner proteins after heat stress, indicating a stress-dependent functional switch of GRXS17 that could contribute to protecting cells from heat stress damage.

RESULTS

GRXS17 releases its Fe-S cluster and oligomerizes under combined oxidative and heat stress

When purified under anaerobic conditions, GRXS17 adopts a dimeric form coordinating up to three Fe-S clusters together with six molecules of GSH (Knuesting et al., 2015). As Fe-S clusters are sensitive to oxidation, we sought to examine the structural modifications of GRXS17 upon transfer to aerobic conditions. As expected, the anaerobically reconstituted GRXS17 Fe-S cluster shows a circular dichroism (CD) spectrum typical for the presence of [2Fe-2S] clusters (Figure 1A). When exposed to air, the spectral footprint of the Fe-S cluster was progressively destabilized by oxygen and finally lost, confirming the sensitivity of the Fe-S cluster to oxidation (Figure 1A).

In parallel to the loss of the Fe-S cluster, a size-exclusion chromatography (SEC) assay revealed a progressive shift of GRXS17 to a high-molecular weight (HMW) form of >250 kDa after 3 h of exposure to air. After 12 h, a HMW complex of a higher range was observed (Figure 1B). Similar data were observed by native gel electrophoresis and non-reducing SDS-PAGE (Figure 1E-F). As expected, holo-GRXS17 migrates, on non-reducing native gel, as a single band likely corresponding to a dimeric form. However, after storage under aerobic conditions for more than 12 h, oligomers were formed, underscoring the high sensitivity of holo-GRXS17 to oxygen (Figure 1E-F). All in all, we showed that the presence of the Fe-S cluster prevents the oligomerization of GRXS17.

To further examine the stability of the Fe-S cluster under oxidative conditions, we exposed the holoGRXS17 to physiological concentrations (0.2-1 mM) of H_2O_2. As previously shown (Knuesting et al., 2015), the UV-VIS spectrum of the reconstituted GRXS17 exhibited absorbance peaks at 320 and 410 nm, characteristic for [2Fe-2S] clusters. Upon H_2O_2 treatment, the Fe-S cluster is lost in a dose-dependent manner (~50% loss in 12 and 5 min at 0.2 mM and 1 mM, respectively), confirming the sensitivity of the Fe-S cluster to oxidation (Figure 1C-D). As high temperature was previously shown to destabilize Fe-S clusters in other proteins (Yan et al., 2013), we also monitored its stability at high temperatures. Both 35°C and 43°C temperatures had little effect on the stability of the cluster after short-term treatments, indicating that the Fe-S cluster is not heat sensitive (Figure 1C-D and Supplemental Figure 2). However, when combining H_2O_2 treatment with a physiological high-temperature of 35°C, an accelerated loss of the Fe-S cluster (~50% loss in 3 min

at 0.2 mM H_2O_2) was observed, showing that higher temperatures potentiate the oxidative effect on Fe-S cluster stability. As expected, extensive oligomerization of GRXS17 was observed by native gel and non-reducing SDS-PAGE gels after H_2O_2 treatment, while high temperature exposure had less impact on oligomerization of GRXS17 (Figure 1E-F).

GRXS17 oligomerizes through intermolecular disulfides and noncovalent interactions

We further explored GRXS17 oligomerization after loss of Fe-S clusters using SEC (Figure 2). As expected, HMW complexes (~900-1000 kDa) were observed in the native apoGRXS17 (Figure 2A, blue line). When separating these fractions on a non-reducing SDS-PAGE gel, a laddering profile was observed, suggesting that the HMW complexes are partially dissociated by SDS and that the remaining HMW bands contain disulfide-linked GRXS17 oligomers (Figure 2D). These data indicate that native GRXS17 oligomerizes through non-covalent interactions and intermolecular disulfides. Consistently, incubation of the native GRXS17 with dithiothreitol (DTT) prior to SEC led to a decrease of the ~900-1000 kDa peak and a concomitant increase of the 110 kDa peak, likely corresponding to homodimeric GRXS17 (Figure 2A). Furthermore, non-reducing SDS-PAGE analyses indicated that the peaks corresponding to oligomeric and dimeric GRXS17 consist of non-covalently interacting monomers (Figure 2D).

To analyze the role of the active-site cysteines on oligomerization, mutated forms of GRXS17 were separated by SEC. Interestingly, the TRX-domain C33S mutant behaved similarly to reduced wild-type GRXS17 (Figure 2B and Supplemental Figure 1), namely exhibiting comparable peaks at ~900-1000 kDa and 110 kDa. Moreover, the distribution between these peaks was not influenced by DTT treatment prior to SEC, indicating that Cys33 plays a major role in the oligomerization, very likely by forming intermolecular disulfide bonds (Figure 2B). Non-reducing SDS-PAGE analyses of the SEC fractions confirmed this statement, as only monomers were found in both conditions (Figure 2E). Strikingly, mutation of all active site cysteines completely abolished oligomerization,

as GRXS17-C33/179/309/416S exclusively eluted as a dimer (Figure 2C and Supplemental Figure 1). Again, only monomers were found in non-reducing SDS-PAGE, indicating that the dimeric apo-GRXS17 is likely formed by non-covalently interacting (Figure 2F).

To further investigate the reduction mechanism of the intermolecular disulfide bonds-mediated oligomeres, we used a physiological disulfide bond reduction system (NADPH/NTRA/TRXh5) located in the cytosol (Reichheld et al., 2007). Interestingly, incubating GRXS17 oligomers with the complete TRX system partially restored monomers, suggesting that at least *in vitro*, GRXS17 covalent oligomers are reduced by the TRX system (Figure 2G).

Finally, to verify the impact of Cys mutations on the GRXS17 structure, we analyzed secondary structure changes of GRXS17 and GRXS17-C33/179/309/416S with CD spectroscopy (Supplemental Figure 3). The general structure (α-helices, β-strands and turn) remained similar between both proteins, indicating that the C33/179/309/416S mutations do not induce major secondary structure changes of GRXS17. The effect of Cys oxidation on the conformation of GRXS17 was also determined. Treatment with 400 µM H_2O_2 resulted in a minor change in secondary structure composition of wild-type GRXS17, but not for the GRXS17-C33/179/309/416S variant (Supplemental Figure 3A). This minor change in secondary structure composition of GRXS17 upon oxidation can correspond to either a local or a global conformational change, which is likely to involve the partial unfolding of α-helices and the formation of β-strands (Supplemental Figure 3B). As this conformational change was not observed for the quadruple Cys variant GRXS17-C33/179/309/416S, we can conclude that this structural change depends on the oxidation of the catalytic cysteines and the formation of disulfide bonds in wild-type GRXS17.

To summarize, we showed that recombinant GRXS17 is able to oligomerize by forming intermolecular disulfides in which the active site C33 of the TRX-domain plays a major role, and which can be reduced *in vitro* by the TRX system. In addition to being involved in Fe-S cluster coordination, C179, C309 and C416 seem to be important for maintaining non-covalent interactions

between protomers. Finally, the active site residues C33, C179, C309 and C416 are not involved in the dimer structure, which likely relies on non-covalent interactions.

A holo-apo redox switch of GRXS17 activates holdase activity upon oxidation

Molecular chaperone activities are often associated with oligomerization and are related to thermotolerance (Lee et al., 2009). Therefore, the potential role of GRXS17 as a molecular chaperone was analyzed using different chaperone substrates. To monitor holdase activity, we used the Arabidopsis cytosolic malate dehydrogenase (MDH1, EC 1.1.1.37) and the porcine heart mitochondrial citrate synthase (CS, EC 4.1.3.7) as client proteins (Figure 3 and Supplemental Figure 4). We analyzed the effect of GRXS17 on the high-temperature-induced aggregation of MDH and CS, a classical assay to monitor the activity of molecular chaperones *in vitro* (Voth et al., 2014). Incubation of MDH or CS with reduced or oxidized apo-GRXS17 prevented thermal aggregation at 55°C and 43°C, respectively (Figure 3A and Supplemental Figure 4). Increasing the apo-GRXS17/MDH ratio progressively decreased MDH aggregation which was fully prevented at a molar ratio of 1:1 apo-GRXS17:MDH (Figure 3B). Notably, this effect was stronger than described for holdases from various organisms (e.g., HSP33, Get3, CnoX, TDX; Jakob et al., 1999; Lee et al., 2009; Voth et al., 2014; Goemans et al., 2018). In contrast, in the absence of GRXS17 or in the presence of an excess of ovalbumin, MDH or CS significantly aggregated after 15 min (Figure 3A-B). Interestingly, a comparable holo-GRXS17/CS ratio did not prevent CS aggregation, indicating that the holdase activity of GRXS17 is specifically associated with the apo-GRXS17 form (Figure 3A). Subsequently, we verified that the Fe-S cluster in the holo-GRXS17 is stable at 43°C (Supplemental Figure 2). Notably, holo-GRXS17 holdase activity could not be measured using MDH because of the instability of the Fe-S cluster at 55°C (Supplemental Figure 2).

We also monitored the foldase activity of GRXS17 using glucose-6-phosphate dehydrogenase (G6PDH) as a substrate. To distinguish between foldase and disulfide reductase activities, we used urea-denatured Cys-free G6PDH from *Leuconostoc mesenteroides* (G6PDH, EC 1.1.1.49).

Increasing the apo-GRXS17:G6PDH ratio progressively restored the G6PDH activity (Figure 3C-D). This reactivation was faster in the presence of GRXS17, reaching nearly 36% recovery after 3 h at a quite high 10:1 ratio of GRXS17:G6PDH (Figure 3D). Reduced or oxidized holo-GRXS17 similarly restored G6PDH activity, indicating that the foldase activity of GRXS17 is independent of the presence or absence of the Fe-S cluster (Figure 3C-D). We also showed that these activities are ATP-independent (Supplemental Figure 5). Collectively, our data show that GRXS17 can adopt both a holdase and a slight foldase activity *in vitro,* and that the holdase activity is specific for the apo-form.

Oligomerization determines the holdase activity of GRXS17

The capacity of apo-GRXS17 to oligomerize depends on both disulfide bonds involving active site Cys residues and non-covalent electrostatic interactions (Figure 2). To uncover forms that are associated with chaperone activity, we tested the chaperone activity of the Cys/Ser-variants of GRXS17 using MDH as substrate (Figure 4A). We found that GRXS17(C33S), which does not abolish oligomerization state, had holdase activity (Figure 2C and Figure 4A). However, in the oligomerization-abolished GRXS17-C33/179/309/416S variant (Figure 2D) no holdase activity was observed (Figure 4A). This suggested that the holdase activity depends on the presence of the active-site cysteines. To further demonstrate that oligomerization is required for holdase activity, we incubated reduced and oxidized apo-GRXS17 with a low concentration of the chaotropic agent guanidinium hydrochloride (GdnHCl), which abolishes weak-bonds like hydrophobic and electrostatic interactions (Figure 4B). We found that the holdase activity of reduced GRXS17 is inhibited with GdnHCl, while the holdase activity of oxidized GRXS17 is preserved. Finally, we tested the role of the cysteines in GRXS17 foldase activity (Figure 4C). We found that GRXS17 Cys mutations do not negatively affect GRXS17 foldase activity, suggesting that disulfide-linked oligomerization is not required for its foldase activity.

GRXS17 is involved in tolerance to moderate heat stress

To reveal the physiological significance of the redox-dependent chaperone activity of GRXS17, we explored the possible role of GRXS17 in plant thermotolerance. Therefore, we subjected *grxs17* mutant plants to different heat-stress regimes (Yeh et al., 2012). The impact of heat stress on shoot meristem viability was first quantified by monitoring the appearance of new leaves. The viability of the *grxs17* mutant was similar to wild-type plants for both Short-term Acquired Thermotolerance (SAT) and Long-term Acquired Thermotolerance (LAT) regimes (Figure 5A-B). In contrast, a mutant lacking the heat-shock protein 101 (HSP101) chaperone was hypersensitive to SAT and LAT regimes (Yeh et al., 2012), indicating that GRXS17 is not involved in SAT and LAT (Figure 5A-B). However, compared to wild-type plants, *grxs17* mutants were significantly more sensitive to a moderate heat stress regime (TMHT: Tolerance to Moderated High Temperature; Figure 5C), indicating that GRXS17 is specifically involved in the response to this heat stress regime. The thermosensitive phenotype of *grxs17* was fully complemented by constitutively overexpressing the full-length GRXS17:GFP fusion under the control of the 35S CaMV promoter, indicating that the TMHT phenotype of *grxs17* is due to the loss of the GRXS17 function and that, neither the attached GFP nor the constitutive overexpression under a strong promoter, perturb the complementation functions (Figure 5C-D and Supplemental Figure 6). Importantly, the overexpression of the GRXS17-C33S:GFP fusion restored the wild-type phenotype, while the expression of the GRXS17-C33/179/309/416S:GFP variant failed to complement the mutant phenotype (Figure 5C-D, Supplemental Figure 6). This last observation demonstrates the role of active site Cys in moderate heat stress tolerance.

To study the impact of high temperature on roots, we performed a similar experiment by following the root development after the TMHT regime (Figure 6). Plants were grown at 20°C for 6 days before the temperature was shifted to 30°C. For root growth, 30°C was used instead of 35°C because this latter temperature affected root growth of plants from all genotypes (Supplemental Figure 7). The primary root of wild-type seedlings grew similarly after the 30°C temperature shift

compared to plants continuously grown at 20°C (Figure 6A-B). While root growth of the *grxs17* mutant was slower than the wild-type at 20°C, it almost completely stopped after the 30°C shift, confirming the role of GRXS17 in root growth which is exacerbated at higher temperature. When the *grxs17* mutant was complemented with the GRXS17-GFP fusion protein, the mutant behaved like wild-type in both conditions. However, GRXS17-C33/179/309/416S:GFP failed to complement the *grxs17* mutant, pointing to the role of these Cys in root growth (Figure 6A-B). The size of the root apical meristem (RAM) was observed after 12 days of growth at 20°C or after the shift to 30°C (Figure 6C-D). The size of the RAM associated with the primary root growth, being slightly smaller at 20°C in both in the *grxs17* and the *GRXS17-C33/179/309/416S:GFP*-complemented lines, and strongly decreased at 30°C (Figure 6C-D and Supplemental Figure 8). This shows a high impact of heat stress on the meristematic activity of the mutant.

To characterize other root growth parameters, we also estimated the role of GRXS17 in lateral root (LR) development. While LR density was not affected at 20°C in any of the studied genotypes, it markedly decreased in the *grxs17* and the *GRXS17-C33/179/309/416S:GFP*-complemented lines at 30°C (Figure 6E).The density of lateral root primordia (LRP; i.e. early stage of LR not emerged from the root cortex) increased in the same genotypes, suggesting that high temperature does not inhibit initiation of LR but rather elongation in the mutant and *GRXS17-C33/179/309/416S:GFP*-complemented lines (Figure 6F). Propidium iodide (PI) staining was used to monitor cell death in meristematic zones (Truernit and Haseloff, 2008). While we did not observe cell death in the RAM in any conditions and genotypes (Figure 6D and Supplemental Figure 8), cell death was observed in the LRP in *grxs17* (Figure 6G). This suggests that GRXS17 prevents heat stress injuries at an early stage of LR development, supporting the LR elongation inhibition at 30°C. Indeed, the role of GRXS17 in early meristem establishment was also observed when the *grxs17* mutant seeds were subjected to high temperature at 28°C. While the mutant seeds germinated properly, they stopped growing at early plantlet stage and harbored a very short root. Importantly, the structure of the RAM looked disorganized and showed cell death (Supplemental Figure 9).

Altogether, these results highlight the role of GRXS17 in the tolerance of plants to moderate heat stress, acting to protect both shoot and root meristems. Importantly, the active site cysteines of GRXS17 seem to play an essential role in root growth and thermotolerance.

GRXS17 oligomerizes *in planta* and associates with a different set of proteins upon shifting to a higher temperature

In addition to *in vitro* assays, we also explored GRXS17 oligomerization *in vivo*. Total soluble protein extracts prepared from Arabidopsis seedlings grown at standard temperature (20°C) and exposed to heat stress (35°C for 2 h) were fractionated by SEC (Figure 7 and Supplemental figure 10). Immunoblot analyses of eluted fractions revealed a peak containing GRXS17 eluting at ~100–150 kDa (lanes 23–25), corresponding to a molecular weight of a GRXS17 dimeric form (~110 kDa; Knuesting et al., 2015). Moreover, at 20°C, a GRXS17 signal was also detected in fractions (lanes 18–21) corresponding to an HMW (~380 kDa) form (Figure 7 and Supplemental figure 10). Interestingly, plants subjected to heat stress accumulated higher levels of HMW forms eluting in the range from SEC column (lanes 16-18), corresponding to 520 kDa (Figure 7). These data suggest that similarly to *in vitro* analyses (Figure 1 and 2), GRXS17 forms HMW-complexes *in vivo*, although the sizes of these complexes are not fully similar. Also, we cannot rule out that GRXS17 oligomers associate with other proteins.

Finally, we sought to identify GRXS17 partners using immunoprecipitation coupled to mass-spectrometry determination (IP-MS). To this end, *grxs17* mutant plants were transformed with a *Pr35S:GRXS17:FLAG-HA* construct. The expression of the construct was verified by immunoblotting and its functionality was assessed by complementation of the phenotype under TMHT (Supplemental Figure 11). Total protein extracts from GRXS17:FLAG-HA-expressing plants grown at 20°C or shifted for 2 h to 35°C were collected for IP-MS analyses. Non-specific GRXS17 contaminants were identified within the same experiments using *grxs17* mutant plants expressing a GRXS17 protein devoid of the FLAG-tag. We employed a label-free quantitative

proteomic approach to identify proteins significantly enriched after IP by comparison with the control samples. Five biological replicates were analyzed by mass spectrometry after FLAG immunoprecipitation from total protein extracts of plants expressing GRXS17:FLAG-HA or non-tagged GRXS17 (control) grown at 20°C or shifted for 2 h to 35°C. GRXS17 was the only protein significantly enriched in the tagged samples after IP ($P<0.05$, Bonferroni corrected Student's t-test). In addition, we identified 23 proteins from plants grown at 20°C and 12 proteins from plants shifted to 35°C that were present and quantified in at least 3 of the 5 replicates from the tagged strain and not found in any of the 5 replicates from control non-tagged plants (Table 1). Using this all-or-nothing approach (i.e. considering only proteins totally absent in control plants), several likely interactants, such as the redox-related enzymes protein disulfide isomerase (PDIL1-4) and monodehydroascorbate reductase (MDAR2), were identified at 20°C. As suggested by the predicted subcellular localization, all partners identified are not presumably direct interactants of GRXS17 in the cell (Table 1). While protein domains common between BolA1 and BolA2 likely mediate the interaction with GRXS17 (Couturier et al., 2014), the interaction with BolA1 located in chloroplasts may not be physiologically relevant. A different set of interaction partners was identified after a 2 h temperature shift from 20°C to 35°C, and only 4 proteins were identified in both conditions (Table 1). Among them, the nucleo-cytoplasmic BolA2 was always present (Supplemental Table 1). This interaction is consistent with previous studies that report the interaction of GRXS17 with BolA2 (Couturier et al., 2014). Finally, to identify GRXS17 partners in HMW complexes, total protein extracts from plants grown at 20°C or shifted for 2 h to 35°C were first separated by SEC, and HMW fractions containing GRXS17:FLAG-HA were collected for IP-MS analysis. A simple subtractive analysis between the samples failed to identify a similar set of proteins as in the previous approach, suggesting that those proteins are not involved in HMW complexes (Supplemental Table 1). However, BolA2 was identified after IP-MS in HMW fractions, indicating that BolA2 is a major GRXS17 oligomer interactant possibly associated with the molecular chaperone activity of GRXS17.

DISCUSSION

Apo-GRXS17 switches to holdase activity upon stress

During periods of heat stress, living organisms need to rapidly adapt to cope with the damaging effects of increasing temperatures. The sessile nature of plants makes them particularly vulnerable to heat stress. As in other organisms, a set of heat-shock proteins acts as molecular chaperones to prevent damage caused by protein inactivation and aggregation (Hanzén et al., 2016; Hartl et al., 2011). Here, we demonstrated that the Fe-S cluster-harboring GRXS17 becomes a holdase after exposure to heat in oxidizing conditions. This switch happens within minutes by a redox- and temperature-mediated destabilization of the Fe-S cluster, and subsequent disulfide bond formation (Figure 8). The redox-switch of Fe-S cluster-containing GRX has previously been shown to occur under oxidizing conditions in other GRX. In these cases, the active site Cys are involved in the Fe-S cluster which inhibits the thiol-reducing activity with the loss of the Fe-S cluster restoring the activity (Lillig et al., 2005; Berndt et al., 2007; Rouhier et al., 2007; Bandyopadhyay et al., 2008; Riondet et al., 2012). In contrast, the apo-GRXS17 of this study is inactive as a thiol reductase, as also reported for other class-II GRX (Bandyopadhyay et al., 2008; Knuesting et al., 2015; Moseler et al., 2015). This lack of thiol reductase activity may be linked to the specificity of the active site and the low reactivity for GSH (Begas et al., 2017; Liedgens et al., 2020).

Interestingly, the active-site cysteines of GRXS17 are crucial for the holdase redox switch as they coordinate both the Fe-S cluster and respond to an oxidizing environment, such as aerobic conditions, H_2O_2 exposure, or heat stress. As such, GRXS17 may act as a sensor for cellular redox changes. In fact, high temperature by itself does not destabilize the Fe-S cluster, but the simultaneous presence of H_2O_2 oxidatively changes the conformation of the protein and induces oligomerization through non-covalent interactions and disulfides (Figure 8). These observations indicate that the Fe-S cluster stabilizes the dimeric structure of GRXS17, and only after dissociation

the protein can undergo oligomerization. A similar function has previously been shown in Archaea, where the loss of a [4Fe-4S] cluster causes oligomerization of the D subunit of the RNA polymerase (Hirata et al., 2008). In GRXS17, we showed that the active-site cysteines (C33, C179, C309 and C416) are required for both non-covalently- and covalently-mediated oligomerization (Figure 2). Although GRXS17 reduces *in vitro* a monomeric glutathionylated form and a dimeric disulfide-bridged form of BolA2 (Couturier et al., 2014), the oligomerization of the apo-GRXS17 protein under oxidative conditions may inhibit this activity (Ströher et al., 2016).

Proteins that combine chaperone function with a redox activity have been described previously. For example, plant thiol reductase proteins TRXh3, TDX and NTRC exhibit chaperone activities triggered by oxidative stress and heat shock exposure, leading to a shift of the protein structure from low-molecular weight form to HMW complexes (Lee et al., 2009; Park et al., 2009; Chae et al., 2013). Also, overoxidation of nucleophilic cysteine of 2-Cys PRX triggers oligomerization and induces chaperone activity (Liebthal et al., 2018). GRXS17 is different as it has no oxidoreductase activity but has a much more efficient holdase activity than the thiol oxidoreductases (Figure 3 and (Lee et al., 2009; Park et al., 2009; Chae et al., 2013)). Remarkably, the key to induce holdase chaperone activity is the release of the redox-dependent Fe-S cluster. To our knowledge, this is the first example of an FeS protein that turns into a chaperone through a switch between holo- and apo-form. In *Escherichia coli*, a similar example is Hsp33 which coordinates zinc via conserved cysteines (Jakob et al., 1999; Jakob et al., 2000; Winter et al., 2008). Upon oxidation with H_2O_2, disulfide bonds are formed between the coordinating cysteines and zinc is released, activating Hsp33 holdase activity. Here, zinc coordination, oxidation and activation state of Hsp33 are directly linked to the redox state of the environment (Jakob et al., 1999; Jakob et al., 2000; Winter et al., 2008). As another example in yeast, the cytosolic ATPase Get3 turns into an effective ATP-independent chaperone when oxidized (Voth et al., 2014). In yeast also, a redox switch in the peroxiredoxin Tsa1 is required for recruitment of Hsp70 chaperones and the Hsp104 disaggregase to misfolded proteins formed upon H_2O_2 exposure during aging (Hanzén et al., 2016). Furthermore,

the holdase activity of *E. coli* chaperedoxin CnoX is activated by chlorination upon bleach treatment to protect substrates from irreversible oxidation (Goemans et al., 2018). Whether GRXS17 acts by protecting its interactors from overoxidation or to recruit other chaperones to their target proteins remains to be determined.

Our *in vitro* experiments showed that GRXS17 has a slight constitutive foldase activity which is independent of ATP (Supplemental Figure 5). Such activity clearly differs from most *bona fide* prokaryotic (e.g. GroEL-GroES) and eukaryotic foldases (e.g. Hsp70, Hsp90) which need ATP for their foldase activity (Mayer, 2010; Hartl et al., 2011). Nevertheless, a number of chaperones have been identified that promote folding in the absence of high-energy cofactors (Stull et al., 2016; Horowitz et al., 2018). As an example, the small ATP-independent chaperone Spy from *E. coli* uses long-range electrostatic interactions and short-range hydrophobic interactions to bind to its unfolded client proteins and drive their folding (Koldewey et al., 2016).

Protein disulfide isomerase (PDI) and cyclophilin, which catalyzes disulfide formation and isomerization of disulfides, exhibit folding activities through their active site Cys (Park et al., 2013; Ali Khan and Mutus, 2014). GRXS17 functions differently, as the foldase activity of GRXS17 is independent of its active-site cysteines (Figure 4). Nevertheless, two additional cysteines are present in the first and third GRXS17 domains, including Cys470 located in the proximity of the potential glutathione-interacting residue Asp471 and which is also conserved in GRXS14 and GRXS16 but not in GRXS15 (Supplemental Figure 1). Their involvement in GRXS17-foldase activity cannot be ruled out. Future experiments will have to be performed to decipher the mechanistic of the foldase activity of GRXS17.

GRXS17 associates with different proteins under high temperature

In eukaryotic organisms grown under non-stress conditions, the cytosolic compartment is a highly reducing environment (Schwarzländer et al., 2008). However, in heat-stressed plants, intracellular oxidation triggered by Reactive Oxygen Species (ROS) accumulation has been largely documented

(Choudhury et al., 2017; Dickinson et al., 2018). Therefore, in regard to changes in redox status depending on the temperature, it is likely that the major GRXS17 form is the Fe-S cluster-containing dimeric form under standard growth temperatures, but a significant proportion of GRXS17 switches to HMW complexes in plants subjected to heat stress (Figure 7). Although the difference in the size of the HMW complexes observed in recombinant GRXS17 and in plant extracts will require further exploration, the switch to HMW complexes appears to be necessary for plant survival under heat stress. As the *grxs17* mutant is highly sensitive to moderate high temperature regimes, the mutant can only be complemented by the GRXS17-Cys variants that are still able to oligomerize (GRXS17 and GRXS17-C33S) and not by GRXS17-C33/179/309/416S (Figures 5 and 6; Cheng et al., 2011; Knuesting et al., 2015). While our data do not fully demonstrate that the holdase activity is needed for heat tolerance, they clearly show the importance of active site Cys in this function. Moreover, the role of Fe-S clusters in thermotolerance will have to be further studied by generating mutant *grxs17* plants complemented by the GRXS17-C179/309/416S in which only cysteines involved in Fe-S cluster coordination (and not in chaperone activity and oligomerization) are mutated. We unfortunately failed to generate such plants yet.

GRXS17 has been previously proposed to improve thermo-, drought- and oxidative-tolerance by enhancing ROS scavenging capacities and expression of heat-shock proteins. This might occur by modulation of gene expression, enzyme activity or protection of antioxidant enzymes (Wu et al., 2012; Wu et al., 2017; Hu et al., 2017). Our data suggest an additional function of GRXS17 through its chaperone activity. The GRXS17 partner protein identification resulted in a low overlap between proteins immunoprecipitated at 20°C and those identified at a higher temperature, suggesting that the set of interacting proteins changes under heat stress. Although it is tempting to suggest that the proteins we identified in immunoprecipitation experiments are protected by GRXS17, further experiments will need to validate these partners and the biological significance of these interactions. Importantly, our observations showing that GRXS17 maintains plant viability under moderate heat stress conditions and prevents cell death in founder cells of root primordia under high temperature

might indicate a role in protecting key actors of meristem function. Possible candidates that we found in our IP are MPK4, which plays a role in temperature signaling pathways (Zhao et al., 2017), and casein kinase II (CK2), a ubiquitous serine/threonine protein kinase in eukaryotes implicated in multiple developmental and stress-responsive pathways (Mulekar and Huq, 2014; Wang et al., 2014). Whether the GRXS17 chaperone activities are involved in the protection of these proteins *in vivo* will require further investigation.

Finally, we propose that the unique properties of GRXS17 among the redox-regulated chaperones (e.g., 2-Cys PRX, TRXh3 or TDX) comes from its inducible holdase function (i.e. Fe-S cluster release under stress), which is not seen for other heat stress-related chaperones (Stull et al., 2016). Homologs of GRXS17 are present in all plants and in most other organisms (Couturier et al., 2009), and their functions in iron metabolism are well documented (Encinar del Dedo et al., 2015; Berndt and Lillig, 2017). It is likely that the switch to holdase chaperone activity, which we described here, could be conserved among different kingdoms of life. Thus, like some other Fe-S cluster-containing GRX (Lillig et al., 2005; Klinge et al., 2007; Lill, 2009; Berndt and Lillig, 2017), GRXS17 uses this oxidation-induced switch to activate a different functionality, here protecting plants from heat-induced damage.

METHODS

Plant materials and growth conditions

The Arabidopsis (*Arabidopsis thaliana*) *grxs17* (SALK_021301) mutant in ecotype Columbia-0 (Col-0) was previously characterized (Knuesting et al., 2015). Arabidopsis seeds were surface-sterilized for 15 min with ethanol 70% (v/v), rinsed with ethanol 95% and completely dried before use. Sterilized seeds were plated onto ½ MS agar medium (2.2 g/L Murashige and Skoog, 0.5 g/L MES, 1% plant agar (w/v), adjusted to pH 5.8) and stratified 48 h at 4°C in the dark. Seedlings were

grown under 120 µmol.m^{-2}.s^{-1} photosynthetic flux at 20°C and 16 h light/8 h dark cycles. Those growth conditions were systematically used unless otherwise indicated.

Gene cloning, mutagenesis, plasmid construction.

For the construction of transgenic complemented line of the *grxs17* mutant and production of recombinant proteins, cDNA of GRXS17 (At4g04950) was inserted into the pGEM-T Easy plasmid (Promega, Madison, WI, USA). Different point mutations of cysteines to serines in GRXS17 were generated using the QuikChange II Directed Mutagenesis Kit (Agilent) using primers detailed in Supplemental Table 2: GRXS17-C33S and GRXS17-C33S/C179S/C309S/C416S.

To generate complemented lines, *GRXS17*, *GRXS17-C33S*, and *GRXS17-C33S/C179S/C309S/C416S* genes were cloned in the pCAMBIA1302 (*Pr35S:gene:GFP*) vector. To perform immunoprecipitation, *GRXS17* was cloned in a modified pCAMBIA 1300 vector harboring a Flag-Flag-HA-HA sequence fused to the C-terminal end of the protein (*Pr35S:gene:Flag/Flag/HA/HA*).

For the production of the recombinant proteins, GRXS17, GRXS17-C33S, GRXS17-C33/179/309/416S and the cytosolic malate dehydrogenase1 (cytMDH1) from Arabidopsis (At1g04410; Huang et al., 2018) were cloned in the pET16b vector (Novagen; Merck Biosciences) using primers detailed in Supplemental Table 2.

Transformation of plants

Plasmids were transferred into Arabidopsis via *Agrobacterium tumefaciens* strain GV3101 using the described methods (Clough and Bent, 1998). Transformants were selected on ½ MS medium plates containing 50 µg.mL^{-1} hygromycin and checked by PCR using appropriate primers (Supplemental Table 2).

Production and purification of recombinant proteins

All proteins were produced by induction in *Escherichia coli* BL21(DE3). Cultures of 2 L of a ampicillin-resistant (100 mg.mL^{-1}) colony were grown at 37 °C and induced by 100 µM isopropyl-β-D-galactopyranoside (IPTG) in the exponential phase (DO=0.5). Bacteria were harvested by centrifugation 3 h after induction and stored at -80°C before protein extraction. Pellets were resuspended in buffer (50mM Tris-HCl pH 7.0, 100 mM NaCl, and 1 tablet anti-protease cocktail (Roche) for 25 mL), extracted using a cell disrupter (Constant Systems Limited, Northants, UK) and purified with a commercial kit according to the manufacturer's instructions (His-bind buffer kit, Millipore).

For the GRXS17 reduction assay by the TRX system, 5 µM recombinant GRXS17 protein was incubated in Tris-HCl buffer (50 mM, pH 7.0) for 1 h at 30°C in the presence or absence of NADPH (150 µM), recombinant thioredoxin reductase A (NTRA, 0.8 µM)) and thioredoxin h5 (TRXh5, 0.08 and 0.8 µM) from Arabidopsis (Huang et al., 2018) and dithiothreitol (DTT, 50 mM). Reactions were stopped by addition of non-reducing Laemli buffer, followed by SDS-PAGE gel migration.

In vitro characterization of holo-GRXS17

Chemical reconstitution of holo-GRXS17 was performed under strictly anaerobic conditions in an anaerobic vinyl tent (COY Laboratory Products, Grass Lake, U.S.A.) according to Freibert et al. (2018). In brief, 100 µM GRXS17 were reduced in reconstitution buffer (50 mM Tris-HCl, pH 8, 150 mM NaCl, 10% glycerol (v/v)) in the presence of 2 mM GSH and 2 mM DTT for 3 h at room temperature. For reconstitution, the GRXS17 concentration was diluted to 20 µM and ferric ammonium citrate was added to a final concentration of 400 µM. After 5 min of incubation, lithium sulfide (400 µM) was added followed by a 3 h incubation. Excess iron ammonium citrate and lithium sulfide were removed by desalting using a NAP™ 25 column (GE Healthcare). Subsequently, the Iron-Sulfur Cluster (ISC) were characterized using a CD-spectrophotometer (J-815, Jasco). The reconstituted GRXS17 was transferred to a sealed CD cuvette. Oxidative treatment

559 of the holo-GRXS17 was performed with oxygen (21%) for the indicated time. The analytical SEC
560 was carried out under strict anaerobic conditions. The gel filtration was performed with the ÄKTA
561 Prime Plus System (GE Healthcare) coupled to a Superdex200 10/300 GL column (GE Healthcare).
562 In each case, 50 µg of GRXS17 was applied into the equilibrated column (50 mM Tris-HCl pH 8,
563 150 mM NaCl, 10% glycerol (v/v)) and separated at a flow rate of 0.5 mL/min. The column was
564 calibrated with the Molecular Weight standard 29-669 kDa (Sigma-Aldrich).
565
566 **Holdase and foldase activities**
567 The holdase chaperone was examined using malate dehydrogenase (MDH) or citrate synthase (CS)
568 assays. The cytosolic MDH1 (cytMDH1) from Arabidopsis (Huang et al., 2018) was used instead of
569 commercial MDH, and the protocol from Lee et al. (2009) was slightly adapted with a temperature
570 of 55°C.
571 The CS from porcine heart (EC 4.1.3.7, Sigma-Aldrich) was examined at 43°C according to Sun et
572 al. (2004). The foldase chaperone was examined by using the *L. mesenteroides* glucose-6-phosphate
573 dehydrogenase (G6PDH; EC 1.1.1.49, Sigma-Aldrich) according to Lee et al. (2009). Light
574 scattering (holdase) or absorption (foldase) were monitored with a Shimadzu UV-1800
575 spectrophotometer at 340 nm (Shimadzu) equipped with a thermostated cell holder.
576
577 **Confocal Laser-Scanning Microscopy, cell death observation and root architecture**
578 **measurements**
579 Confocal microscopic observations were carried out using the Axio observer Z1 microscope with
580 the LSM 700 scanning module and the ZEN 2010 software (Zeiss). GFP and propidium iodide (PI)
581 were excited using the 488nm argon-ion laser and collected at 500-550 nm (GFP) or 600-656 nm
582 (PI). Excitation of roGFP2 was performed at 488 and 405 nm and a bandpass (BP 490-555 nm)
583 emission filter was used to collect roGFP2 signal. For background subtraction, signal was recovered
584 using a BP 420-480 nm emission filter during excitation at 405 nm. Image analyses and

quantifications were performed as previously described (Schwarzländer et al., 2008), using the public domain image analysis program ImageJ 1.52i (https://imagej.nih.gov/ij/). For measurement of cell death in roots, seedlings were stained with 100 µg.mL^{-1} PI (Sigma-Aldrich) for 5 min before imaging.

Measurements of RAM length and LRP counting were performed by confocal microscopic observations after PI staining. RAM length was determined by the distance from the quiescent center to the region where endodermis cells were elongating (Truernit and Haseloff, 2008). Measurements of primary root elongation was performed using the NeuronJ software as described (Trujillo-Hernandez et al., 2020). Counting of LR numbers was performed using a stereomicroscope SMZ18 (Nikon, Japan). LR and LRP density were reported for the entire root length.

Size-exclusion chromatography

Gel filtration experiments were performed using an ÄKTA Fast Protein Liquid Chromatography (FPLC) system (Amersham Biosciences) at 4°C. Absorbance was monitored at 280 nm. The column was calibrated using a molecular weight standard (29-669 kDa). For recombinant GRXS17 (wild-type and mutated forms), a Superose 6 column was used, equilibrated with a 50 mM Tris-HCl (pH 7.5) buffer containing 150 mM NaCl and 5 mM $MgCl_2$ at a flow rate of 0.5 ml.min^{-1}. All recombinant protein samples were dialyzed before application. For reducing conditions, samples were incubated with 100 mM of DTT and dialyzed against the above-described buffer supplemented with 5 mM of DTT to maintain the proteins in their reduced state.

For separation of total proteins extracts, a HiPrep column Sephacryl S-300 HR (GE Healthcare Life Sciences) was used and equilibrated with a 50 mM Tris-HCl (pH 7.5) buffer containing 150 mM NaCl, 5 mM $MgCl_2$, 10% (v/v) glycerol and 0.1% (v/v) NP40 at a flow rate of 0.5 ml.min^{-1}. Samples were extracted in the same buffer containing 10 µM of MG132 and 1 tablet per 10 mL

anti-protease cocktail (Roche). Extraction was carried out with a ratio of 1 g of plant powder in two volumes of buffer.

Protein separation by gel electrophoresis and immunoblotting

Precast SDS-PAGE or native gels were used according to the manufacturer's instructions (Biorad). For immunoblot analysis, gels were transferred to nitrocellulose membranes. Rabbit polyclonal antibodies against GRXS17 (1:25,000) were used for protein immunoblotting. Goat anti-rabbit antibodies conjugated to horseradish peroxidase (1:10,000) were used as secondary antibodies and revealed with enhanced chemiluminescence reagents (Immobilon Western Chemiluminescent HRP Substrate, Millipore).

Thermotolerance assays

For the thermotolerance assays, three different protocols were applied: LAT (Long-Term Acquired Thermotolerance), SAT (Short-Term Acquired Thermotolerance) and TMHT (Thermotolerance to Moderately High Temperatures) as defined by Yeh et al. (2012). The seeds were germinated and grown in horizontal plates containing medium MS (4.4 g/L Murashige and Skoog, 1% (w/v) sucrose, pH 5.8). The percentage of viability was calculated by counting the plants that recovered leaf growth after heat stress. For examining the impact of heat stress on roots, seeds were grown on vertical plates and root growth was daily measured using ImageJ.

Immunoprecipitation

Proteins from plants expressing the *Pr35S:GRXS17-Flag/HA* or the *Pr35S:GRXS17* constructs were used for immunoprecipitation experiments. Seeds were germinated and grown in vertical plates containing medium ½ MS during 14 days at 20°C and treated or not for 2 h at 35°C. The proteins were extracted and submitted to immunoprecipitation. Agarose beads with covalently attached anti-Flag antibody were used according to manufacturer's instructions, and bound proteins were eluted

with 0.1 M glycine pH 2.5. In another set of experiments, proteins extracts were first submitted to SEC as described previously. Fractions 18-21 corresponding to oligomers for plants grown at 20°C and fractions 16-19 for plants treated 2 h at 35°C (see Figure 2) were collected and subjected to immunoprecipitation.

Quantitative Mass Spectrometry Analyses

Chemicals and enzymes: Proteomics grade Trypsin and ProteaseMax surfactant were purchased from Promega (Charbonnieres, France). Reversed-phase C18 spin columns, precolumns, and analytical columns were all obtained from Thermo Scientific (Les Ulis, France). Solvents and ion-pairing agents were certified LC-MS grade, and all other chemicals were purchased from Sigma-Aldrich (Saint-Quentin Fallavier, France) with the highest purity available.

Sample preparation: Immunoprecipitated samples were incubated in the presence of 0.02% (v/v) ProteaseMax with 5 mM DTT for 20 min at 40°C. Free cysteines were further carbamidomethylated by adding 11 mM iodoacetamide for 30 min at room temperature in darkness. Proteins were digested overnight at 35°C with modified porcine trypsin in a 1:50 (w/w) enzyme:substrate ratio. The digestion was stopped by the addition of 0.1% trifluoroacetic acid, and peptide mixtures were centrifuged for 10 min at 21,500*xg* at 4°C. Tryptic peptides present in supernatants were then subjected to desalting using reversed-phase C18 spin columns as recommended by the supplier. After elution, desalted peptides were concentrated with a SpeedVac (Eppendorf) and 3% (v/v) acetonitrile, 0.1% (v/v) formic acid (solvent A) were added to obtain a final protein concentration of 0.27 µg/µL based on the initial concentration.

Mass spectrometry: Peptide mixtures were analyzed on a Q-Exactive Plus (Thermo Fisher Scientific, San José, CA, USA) coupled to a Proxeon Easy nLC 1000 reversed-phase chromatography system (Thermo Fisher Scientific, San José, CA, USA) using a binary solvent system consisting of solvent A and solvent B (0.1% FA in ACN). Three microliters (800 ng) of tryptic digests was loaded on an Acclaim Pepmap C18 precolumn (2 cm x 75 µm i.d., 2 µm, 100 A)

equilibrated in solvent A, and peptides were separated on an Acclaim Pepmap C18 analytical column (25 cm x 75 µm i.d., 2 µm, 100 A) at a constant flow rate of 250 nL/min by two successive linear gradients of solvent B from 0% to 25% in 100 min, from 25% to 40% in 20 min and then up to 85% in 2 min followed by an isocratic step at 85% for 7 min. The instrument was operated in positive and data-dependent acquisition modes with survey scans acquired at a resolution of 70,000 (at m/z 200 Da) with a mass range of m/z 375-1,400. After each full-scan MS, up to 10 of the most intense precursor ions (except +1, +5 to +8 and unassigned charge state ions) were fragmented in the HCD cell (normalized collision energy fixed at 27) and then dynamically excluded for 60 s. AGC target was fixed to $3x10^6$ ions in MS and 10^5 ions in MS/MS with a maximum ion accumulation time set to 100 ms for MS and MS/MS acquisitions. All other parameters were set as follows: capillary temperature, 250°C; S-lens RF level, 60; isolation window, 2 Da. Acquisitions were performed with Excalibur software (Thermo Fisher Scientific, San José, CA, USA) and to improve the mass accuracy of full-scan MS spectra, a permanent recalibration of the instrument was allowed using polycyclodimethylsiloxane $(C_2H_6SiO)_6$, m/z 445.12003 Da) as lock mass.

Proteomic data processing: MS raw data of HMW complexes were processed with ProteomeDiscoverer 2.2 (Thermo Fisher Scientific, San José, CA, USA) and searched against the UniprotKB Arabidopsis database (25/10/2015; 31480 entries) combined with a database of classical contaminants using an in-house Mascot search server (Matrix Science, London, UK; version 2.4). Mass tolerance was set to 10 ppm for the parent ion mass and 20 mmu for fragments, and up to two missed cleavages per tryptic peptide were allowed. Methionine oxidation, deamidation of asparagine and N-terminal acetylation were taken into account as variable modifications and cysteine carbamidomethylation as a fixed modification. Peptide and protein False Discovery Rates (FDRs) were determined by searching against a reversed decoy database. Peptide identifications were filtered at 1% FDR using the Percolator node. Proteins were filtered at 1% FDR and reverse and contaminants proteins were removed.

MS raw data were processed with MaxQuant software (version 1.6.0.13) and with the associated Andromeda search engine using the UniprotKB Arabidopsis database (25/10/2015; 31480 entries) combined with the MaxQuant database of common contaminants. First and main searches were performed with precursor mass tolerances of 20 and 4.5 ppm, respectively. The minimum peptide length was set to seven amino acids and specificity for protein digestion was restricted to trypsin/P cleavage with a maximum of two missed cleavages per peptides. Methionine oxidation and N-terminal acetylation were specified as variable modifications, and carbamidomethylation of cysteines was specified as a fixed modification. The peptide and protein false discovery rate (FDR) was set to 1%. To increase protein identification, a match between runs was systematically performed (Match time window 0.7 min; alignment time window: 20 min), and for label-free quantification of immuno-precipitated proteins, the LFQ algorithm and normalization were chosen and unique and razor peptides were used.

MaxQuant output was further processed and analyzed using Perseus software (version 1.6.07). Protein quantification was performed using the ProteinGroups.txt file after removing reverse and contaminant proteins and the Log2 transformation of quantitative data. Proteins showing at least two unique and razor peptides and having quantitative data in at least three biological replicates were considered for statistical analysis of each temperature condition using a Benjamini-Hochberg-corrected Student's t-test. Proteins showing a FDR < 0.05 were considered significantly enriched. For both temperature conditions, proteins having quantitative data in biological samples expressing the tagged GRXS17 but not in the five corresponding control samples were treated separately. In this case, only proteins showing quantitative data in three out of the five biological replicates with at least two unique and razor peptides from samples expressing tagged GRXS17 were considered as significant.

Circular Dichroism

712 In preparation for CD analysis, samples of GRXS17 were buffer-exchanged into 20 mM sodium
713 phosphate, 100 mM NaF, pH 7.3, using Bio-Spin® 6 columns, adjusted to 4 μM, and treated with
714 400 μM of either TCEP or H_2O_2 for 1 h at 25°C. Samples were centrifuged and vacuum-degassed
715 for 10 min prior to analysis by CD. CD spectra were collected at 20°C using a J-715
716 spectropolarimeter (JASCO) with a 0.1 mm path-length cuvette, from a range of 250-185 nm in 1.0
717 nm sampling and spectrum averaged over 8 repeats. The spectra of the buffer alone with
718 TCEP/H_2O_2 was subtracted prior to the conversion of data to units of mean residue ellipticity.
719 Secondary structure content was estimated using the online server, BeStSel (Micsonai et al., 2015).
720 For monitoring change in secondary structure over time, CD spectra of 250-190 nm were collected
721 at 100 nm min^{-1}. The secondary structure change of GRXS17 following the addition of a 100-fold
722 excess of H_2O_2 was measured as the change in [θ] at 222 nm over a course of 65 min, spectra
723 collected every 41 s. In Prism (GraphPad) a one-phase decay model was fitted to these data, and a
724 rate of conformational change was determined.
725
726 **Accession numbers**
727 Assigned accession numbers for the genes used in this work are as follows: At3g54900 (GRXS14),
728 At3g15660 (GRXS15), At2g38270 (GRXS16), At4g04950 (GRXS17), At1g04410 (cytMDH1).
729
730 **Supplemental Data**
731 **Supplemental Figure S1.** Alignment of type II GRX of Arabidopsis and yeast.
732 **Supplemental Figure S2.** Fe-S cluster stability under increasing temperatures.
733 **Supplemental Figure S3.** CD study of redox-dependent structural changes in GRXS17 and
734 GRXS17-C33/179/309/416S.
735 **Supplemental Figure S4.** Apo-GRXS17 holdase chaperone activity with MDH as substrate.
736 **Supplemental Figure S5.** GRXS17 foldase chaperone activity is independent of ATP.
737 **Supplemental Figure S6.** GRXS17:GFP protein expression in complemented *grxs17* lines.

738 **Supplemental Figure S7.** Primary root growth under 35°C heat stress.

739 **Supplemental Figure S8.** Determination of the root apical meristem size at 20°C.

740 **Supplemental Figure S9.** Cell death in the root apical meristem of *grxs17*.

741 **Supplemental Figure S10.** Complete immunoblots from Figure 7.

742 **Supplemental Figure S11.** GRXS17:FLAG-HA protein accumulation and TMHT response in
743 *grxs17*-complemented lines.

744 **Supplemental Table S1:** Full list of proteins identified by mass spectrometry after co-
745 immunoprecipitation experiments using either high molecular weight complexes (HMW) or total
746 extracts (Total) from Arabidopsis plants as starting materials.

747 **Supplemental Table S2:** Primers used in this study.

748

749 **ACKNOWLEDGMENTS**

750 The authors would like to thank Marion Hamon for technical assistance for mass spectrometry
751 analyses and Dr. Yee-yung Charng (Academia Sinica, Taiwan) for pioneer experiments on heat
752 stress regimes. This work was supported in part by the Centre National de la Recherche
753 Scientifique, by the Agence Nationale de la Recherche (ANR-Cynthiol 12-BSV6-0011 and ANR-
754 REPHARE 19-CE12-0027), by LABEX DYNAMO ANR-LABX-011 and EQUIPEX CACSICE
755 ANR-11-EQPX-0008, notably through funding of the Proteomic Platform of IBPC (PPI). This
756 project was funded through Labex AGRO (under I-Site Muse framework) coordinated by the
757 Agropolis Fondation (Flagship project CalClim, 2016-03). This study is set within the framework
758 of the "Laboratoires d'Excellence (LabEx)" TULIP (ANR-10-LABX-41). Laura Martins and
759 Avilien Dard are supported by a Ph.D. grant from the Université de Perpignan Via Domitia (Ecole
760 Doctorale Energie et Environnement ED305). Work performed in the lab of Joris Messens was
761 supported by the Research Foundation-Flanders Excellence of Science project no. 30829584, the
762 Research Foundation-Flanders grants no. G0D7914N, and the VUB Strategic Research Programme
763 (SRP34). We gratefully acknowledge the Core Facilities of Protein Spectroscopy and Protein

764 Biochemistry of Philipps-Universität Marburg. Work performed in the lab of Renate Scheibe was
765 supported with funds from the DFG (SCHE 217; SPP 1710). Work performed in the lab of Roland
766 Lill was supported by funds from DFG (SPP 1710 and SFB 987).

767

768 **CONFLICT OF INTEREST**

769 We declare no conflict of interest.

770

771 **Table 1 : Proteins interacting with GRXS17 at 20°C or 35°C.**

772 Binding partners of GRXS17 isolated from 10-day-old plantlets grown at 20°C or after 2h heat treatment at
773 35°C are listed. Putative/established subcellular localizations were determined using SUBA4 (Hooper et al.,
774 2017). Common substrates located in the same (*) or in another (#) subcellular compartment as GRXS17 are
775 indicated. For more details, see Supplemental Table S1.
776

UniProtKB Accession	Description (Gene)	TAIR	Established or putative localization
20°C			
Q9ZPH2 *	Monothiol glutaredoxin-S17 (GRXS17)	At4g04950	nucleus/cytosol
Q9FIC3 *	Protein BOLA2 (BOLA2)	At5g09830	nucleus/cytosol
P56804 #	30S ribosomal protein S14, chloroplastic (RPS14)	AtCg00330	chloroplast
Q682I1 #	Protein BOLA1 (BOLA1)	At1g55805	chloroplast
F4III4	Probable ATP synthase 24 kDa subunit (MGP1)	At2g21870	mitochondria
F4JX83	Thylakoid lumenal 17.4 kDa protein (TL17)	At5g53490	chloroplast
O23299	Enoyl-CoA delta isomerase 2 (ECI2)	At4g14430	peroxisome
O80796	Membrane-associated protein (VIPP1)	At1g65260	chloroplast
O80837	Remorin (DBP)	At2g45820	cytosol/plasma membrane
Q39129	Thiosulfate sulfurtransferase 16 (STR16)	At5g66040	chloroplast
Q8LE52	Glutathione S-transferase (DHAR3)	At5g16710	chloroplast
Q93WJ8	Probable monodehydroascorbate reductase (MDAR2)	At5g03630	cytosol
Q9M885	40S ribosomal protein S7-2 (RPS7B)	At3g02560	cytosol
Q9S9M7	Uncharacterized Nuclear protein (At1g16080)	At1g16080	nucleus/chloroplast
F4K0F5	Protein disulfide isomerase-like 1-4 (PDIL1-4)	At5g60640	endoplasmic reticulum
O82326	SWIB/MDM2 domain superfamily protein	At2g14880	chloroplast
P23586	Sugar transport protein 1 (STP1)	At1g11260	cytosol/plasma membrane
Q37165	NAD(P)H-quinone oxidoreductase subunit 1 (NDH1)	AtCg01100	chloroplast
Q39024	Mitogen-activated protein kinase 4 (MPK4)	At4g01370	nucleus/cytosol
Q8GW78	Clp protease-related protein (At4g12060)	At4g12060	chloroplast
Q8LBI1	60S ribosomal protein L5-1 (At L5)	At3g25520	nucleus/cytosol
Q94AI6	Exocyst complex component (SEC6)	At1g71820	cytosol/plasma membrane

Q96514	Cytochrome P450 (P450 71B7)	At1g13110	cytosol/plasma membrane/endoplasmic reticulum
Q93ZY3	Staurosporin and temperature sensitive 3-like A / Dolichyl-diphosphooligosaccharide transferase (STT3A)	At5g19690	endoplasmic reticulum
35°C			
Q9ZPH2 *	Monothiol glutaredoxin-S17 (GRXS17)	At4g04950	nucleus/cytosol
Q9FIC3 *	Protein BOLA2 (BOLA2)	At5g09830	nucleus/cytosol
P56804 #	30S ribosomal protein S14, chloroplastic (RPS14)	AtCg00330	chloroplast
Q682I1 #	Protein BOLA1 (BOLA1)	At1g55805	chloroplast
B9DFC0	Arginase 2 (ARGAH2)	At4g08870	mitochondria
O23157	Maternal effect embryo arrest 59 (MEE59)	At4g37300	nucleus
Q39054	Molybdopterin biosynthesis protein (CNX1)	At5g20990	cytosol
Q5XF82	Jacalin-related lectin 11 (JAL11)	At1g52100	cytosol
Q8L7W0	SH3 domain-containing protein 3 (At4g18060)	At4g18060	cytosol/plasma membrane
Q9MBA1	Chlorophyllide a oxygenase (CAO)	At1g44446	chloroplast
Q9SXE9	Vacuolar calcium-binding protein-related (At1g62480)	At1g62480	nucleus/cytosol
O64816	Casein kinase II subunit alpha (CKA4)	At2g23070	cytosol/nucleus/chloroplast
P52032	Phospholipid hydroperoxide glutathione peroxidase 1 (GPX1)	At2g25080	chloroplast

FIGURE LEGENDS

Figure 1: Fe-S cluster stability and oligomerization of reconstituted GRXS17. (A) Visible circular dichroism (CD)-spectra of reconstituted holo-GRXS17 under reducing conditions (blue) and after oxygen treatment (3h brown; 12h red) at room temperature. (B) Size-exclusion chromatography (Sephacryl S300 HR) under anaerobic conditions with reconstituted GRXS17 after the respective oxygen treatments. (C) Absorption spectra of GRXS17 subjected to H_2O_2 and heat treatments. UV-VIS absorption spectra were measured after *in vitro* reconstitution under anaerobic conditions and after 20 min of treatment with 20°C (blue), GSH at 20°C (2.5 mM orange), H_2O_2 at 20°C (0.2 mM green; 1 mM red), 35°C in presence of 0.2 mM H_2O_2 (black) or without H_2O_2 (light blue). Inset : Absorption at 410 nm of the same samples. Data are means of 3-6 biological repetitions +/- SE. The letters a, b and c indicate significance compared to the control (blue), of $p>0.1$, $p<0.001$, and $p<0.00001$, respectively, by Student's t-test. (D) Kinetics monitoring the

GRXS17 Fe-S cluster stability subjected to the same treatments as in (C). (E-F) Migration of 5 µg of recombinant GRXS17 with or without the cluster in (E) native PAGE or (F) in non-reducing SDS-PAGE gels. M, Molecular marker. HoloGRXS17 (1) was maintained in air for 3h (2) or 12h (3) or treated for 10 min at 35°C (4), with 0.2 mM H_2O_2 (5) or a combination of both treatments (6). Samples were subjected to non-reducing SDS-PAGE and protein bands were stained by Coomassie blue. Each experiment is representative of three biological repetitions.

Figure 2: GRXS17 forms high molecular weight complexes.

(A,B,C) Size-exclusion chromatography (SEC) analysis (Superose 6) of 740 µg (A) GRXS17 protein, (B) GRXS17-C33S and (C) GRXS17-C33/179/309/416S maintained in air after purification. The protein was reduced with 100 mM DTT (red) or without (blue) before loading on the column. Approximative molecular weights were calculated based on the elution volume of reference proteins (see Methods). (D,E,F) Aliquots of elution fraction (30 µL) shown in (A,B,C) were subjected to non-reducing SDS-PAGE. (G) GRXS17 oligomers are reduced by the TRX system. Recombinant GRXS17 (5 µM) was incubated with NADPH (150 µM) for 1h at 30°C, with or without NTRA (0.8 µM), DTT (50 mM) and TRXh5 as indicated in the table. Afterwards, proteins were separated by non-reducing SDS-PAGE.

Figure 3: GRXS17 exhibits holdase and foldase chaperone activities.

(A-B) GRXS17 holdase activity toward citrate synthase (CS; A) or malate dehydrogenase (MDH; B) was measured by light scattering. CS or MDH were incubated alone (Control), with ovalbumin or with the different GRXS17 proteins. (A) Holo-GRXS17 or apo-GRXS17 in their reduced or oxidized forms were incubated with CS at a 1:1 (0.5:0.5 µM) ratio at 43°C. Ovalbumin ratios were 1:1 (0.5:0.5 µM). (B) Ratios of apo-GRXS17/MDH were 0.2:1 (0.1:0.5 µM), 0.5:1 (0.25:0.5 µM) and 1:1 (0.5:0.5 µM). Ovalbumin ratios were 1:1 (0.5:0.5 µM). (C-D) GRXS17 foldase activity was measured by reactivation of the glucose 6-phosphate dehydrogenase (G6PDH) activity after

denaturation with urea. The zero time point represents the starting activity for the reactivation assay with 100% being the activity before heat denaturation. (C) Holo-GRXS17 or apo-GRXS17 in their reduced or oxidized forms were incubated with G6PDH at a 5:1 (0.65:0.13 µM) ratio at 30°C. Ovalbumin ratios were 5:1 (0.65:0.13 µM). D) Ratios of apo-GRXS17/G6PDH were 2:1 (0.26:0.13 µM), 5:1 (0.65:0.13 µM) and 10:1 (1.3:0.13 µM). Ovalbumin ratios were 5:1 (0.65:0.13 µM). Data are means of at least 3 biological repetitions +/- SE. Control and ovalbumin curves are the same and represent means and SD of all experiments (n>9).

Figure 4: Role of GRXS17 active-site cysteines and oligomerization in holdase and foldase activities. (A) Holdase activity of GRXS17 and Cys-mutated GRXS17 proteins was measured toward MDH heat-induced precipitation by light scattering at 55°C. MDH was incubated alone (Control), with ovalbumin or with the different GRXS17 proteins at 1:1 (0.5:0.5 µM) ratios. (B) GRXS17 proteins reduced by 5 mM DTT (yellow) or oxidized with 1 mM H_2O_2 (green) were treated with 20 mM guanidinium hydrochloride (Gua) as a chaotropic reagent (brown and light blue, respectively). MDH was incubated alone (Control) or with ovalbumin. (C) Foldase activity of GRXS17 and Cys-mutated GRXS17 proteins was determined by measuring the glucose-6 phosphate dehydrogenase (G6PDH) activity after denaturation with urea. The zero time point represents the starting activity for the reactivation assay with 100% being the activity before heat denaturation. G6PDH was incubated alone (Control), with ovalbumin or with the different GRXS17 proteins at 5:1 (0.65:0.13 µM) ratios. Data are means of at least 3 biological repetitions +/- SE. Control and ovalbumin curves are the same and represent means and SD of all experiments made (n>9).

Figure 5: GRXS17 is specifically involved in thermotolerance to moderate high temperature. Wild-type plants (Col-0), the *grxs17* knock-out mutant (*grxs17*), the *grxs17* mutant complemented with a *Pr35S:GRXS17:GFP* construct expressing the GRXS17:GFP fusion protein (+GRXS17), the

GRXS17-C33S:GFP protein (+GRXS17-C33S), the GRXS17-C33/179/309/416S:GFP (+GRXS17-C33/179/309/416S) protein, Heat-Shock Factor A1 quadruple knock-out mutant (*hsfA1QK*) or Heat-Shock Protein 101 knock-out mutant (*hsp101*) plants were subjected to different temperature stress regimes : (A) LAT, Long-term Acquired Thermotolerance ; (B) SAT, Short-term Acquired Thermotolerance ; (C) Thermotolerance to Moderate High Temperature (TMHT). do: days old. rec: recovery. Viability of the plants was assessed by recovery of shoot growth. Data are means of 4-10 biological repetitions +/- SE, n = 20-25. The letters a, b and c indicate a significance compared to Col-0, of $p>0.1$, $p<0.001$, and $p<0.00001$, respectively, by Student's t-test. (D) GRXS17 protein expression in complemented *grxs17* lines. Total protein extracts were prepared from 2-week-old plantlets. Protein extracts were separated by SDS-PAGE and probed with antibodies directed against GRXS17. Plants expressing the transgenes at different levels are represented. In Col-0, the 50 kDa signal corresponds to the native GRXS17 protein. In the complemented lines, the 80 kDa signal corresponds to the GRXS17:GFP fusion protein.

Figure 6: GRXS17 is involved in root development under heat stress. Wild-type (Col-0), the *grxs17* knock-out mutant (*grxs17*), the *grxs17* mutant complemented with a *Pr35S:GRXS17:GFP* construct (+GRXS17) and the *Pr35S:GRXS17-C33/179/309/416S:GFP* construct (+GRXS17-C33/179/309/416S) plants were grown 12 days continuously at 20°C or 6 days at 20°C and shifted to 30°C for 6 more days. (A-B) Primary root length of plants grown at 20°C (A) or shifted to 30°C (B). (C) Root apical meristem (RAM) of plants grown at 20°C (white boxplots) or shifted to 30°C (grey boxplots). (D) RAM of plants shifted to 30°C and stained by propidium iodide. RAM length (bidirectional arrows) was determined by the distance from the quiescent center to where endodermis cells were elongating. (E-F) Density (number per cm of primary root) of emerged lateral roots (LR; E) and lateral root primordia (LRP) after growth at 20°C (white boxplots) or shifted to 30°C (grey boxplots). (G) LRP of plants shifted to30°C and stained by propidium iodide. White arrowheads pinpoint cell death in LRP, whereas unfilled arrowheads represent LRP where

cell death did not occur. Data are means of 3 biological repetitions +/- SE, n = 15. The letters a, b and c indicate a significance compared to Col-0, of $p>0.1$, $p<0.001$, and $p<0.00001$ respectively, by Student's t-test.

Figure 7: GRXS17 forms high molecular weight complexes in plant extracts. Size-exclusion chromatography analysis (Sephacryl S300 HR) of crude protein extracts from Arabidopsis seedlings cultivated 14 days at 20°C and further treated for 2 h at 35°C. The GRXS17 protein was detected after immunoblotting and immunodetection using an anti-GRXS17 serum. Numbered lines correspond to the protein fractions. Protein size of the respective fractions was obtained after calibration using marker proteins.

Figure 8: Model of the GRXS17-redox switch. Under reducing conditions, the holo-GRXS17 forms a dimer which coordinates an iron-sulfur cluster (ISC). In this form, GRXS17 can transfer ISC to cytosolic or nuclear target proteins (represented as a green line in the middle of the oligomeric structures). Under oxidative conditions (H_2O_2, O_2, Heat Stress (HS)), ISC are released and GRXS17 switches to an apo-dimeric form with a foldase activity. Dimers can spontaneously associate to oligomeric forms and further oxidation induces oligomeric structure through formation of intermolecular disulfide bonds at active-site Cys residues. In this form, GRXS17 acquires holdase activities and provides thermotolerance. The oligomeric form can be reduced to recover the apo-dimeric GRXS17 and the Fe-S cluster can eventually be reassembled.

Literature Cited

Ali Khan H, Mutus B (2014) Protein disulfide isomerase a multifunctional protein with multiple physiological roles. Front Chem **2**: 70

Banci L, Ciofi-Baffoni S, Gajda K, Muzzioli R, Peruzzini R, Winkelmann J (2015) N-terminal domains mediate [2Fe-2S] cluster transfer from glutaredoxin-3 to anamorsin. Nat Chem Biol **11**: 772–778

Bandyopadhyay S, Gama F, Molina-Navarro MM, Gualberto JM, Claxton R, Naik SG, Huynh BH, Herrero E, Jacquot JP, Johnson MK, et al (2008) Chloroplast monothiol glutaredoxins as scaffold proteins for the assembly and delivery of [2Fe-2S] clusters. EMBO J **27**: 1122–1133

Begas P, Liedgens L, Moseler A, Meyer AJ, Deponte M (2017) Glutaredoxin catalysis requires two distinct glutathione interaction sites. Nat Commun **8**: 14835

Berndt C, Hudemann C, Hanschmann E-M, Axelsson R, Holmgren A, Lillig CH (2007) How does iron-sulfur cluster coordination regulate the activity of human glutaredoxin 2? Antioxid Redox Signal **9**: 151–157

Berndt C, Lillig CH (2017) Glutathione, Glutaredoxins, and Iron. Antioxid Redox Signal **27**: 1235–1251

Chae HB, Moon JC, Shin MR, Chi YH, Jung YJ, Lee SY, Nawkar GM, Jung HS, Hyun JK, Kim WY, et al (2013) Thioredoxin reductase type C (NTRC) orchestrates enhanced thermotolerance to Arabidopsis by its redox-dependent holdase chaperone function. Mol Plant **6**: 323–336

Cheng N-H, Liu J-Z, Liu X, Wu Q, Thompson SM, Lin J, Chang J, Whitham SA, Park S, Cohen JD, et al (2011) Arabidopsis monothiol glutaredoxin, AtGRXS17, is critical for temperature-dependent postembryonic growth and development via modulating auxin response. J Biol Chem **286**: 20398–20406

Choudhury FK, Rivero RM, Blumwald E, Mittler R (2017) Reactive oxygen species, abiotic stress and stress combination. Plant J **90**: 856–867

Clough SJ, Bent AF (1998) Floral dip: a simplified method for Agrobacterium-mediated transformation of Arabidopsis thaliana. Plant J Cell Mol Biol **16**: 735–743

Couturier J, Jacquot J-P, Rouhier N (2009) Evolution and diversity of glutaredoxins in photosynthetic organisms. Cell Mol Life Sci CMLS **66**: 2539–2557

Couturier J, Przybyla-Toscano J, Roret T, Didierjean C, Rouhier N (2015) The roles of glutaredoxins ligating Fe-S clusters: Sensing, transfer or repair functions? Biochim Biophys Acta **1853**: 1513–1527

Couturier J, Ströher E, Albetel A-N, Roret T, Muthuramalingam M, Tarrago L, Seidel T, Tsan P, Jacquot J-P, Johnson MK, et al (2011) Arabidopsis chloroplastic glutaredoxin C5 as a model to explore molecular determinants for iron-sulfur cluster binding into glutaredoxins. J Biol Chem **286**: 27515–27527

Couturier J, Touraine B, Briat J-F, Gaymard F, Rouhier N (2013) The iron-sulfur cluster assembly machineries in plants: current knowledge and open questions. Front Plant Sci **4**: 259

Couturier J, Wu H-C, Dhalleine T, Pégeot H, Sudre D, Gualberto JM, Jacquot J-P, Gaymard F, Vignols F, Rouhier N (2014) Monothiol glutaredoxin-BolA interactions: redox control of Arabidopsis thaliana BolA2 and SufE1. Mol Plant **7**: 187–205

Dickinson PJ, Kumar M, Martinho C, Yoo SJ, Lan H, Artavanis G, Charoensawan V, Schöttler MA, Bock R, Jaeger KE, et al (2018) Chloroplast Signaling Gates Thermotolerance in Arabidopsis. Cell Rep **22**: 1657–1665

Encinar del Dedo J, Gabrielli N, Carmona M, Ayté J, Hidalgo E (2015) A cascade of iron-containing proteins governs the genetic iron starvation response to promote iron uptake and inhibit iron storage in fission yeast. PLoS Genet **11**: e1005106

Frey AG, Palenchar DJ, Wildemann JD, Philpott CC (2016) A Glutaredoxin·BolA Complex Serves as an Iron-Sulfur Cluster Chaperone for the Cytosolic Cluster Assembly Machinery. J Biol Chem **291**: 22344–22356

Goemans CV, Vertommen D, Agrebi R, Collet J-F (2018) CnoX Is a Chaperedoxin: A Holdase that Protects Its Substrates from Irreversible Oxidation. Mol Cell **70**: 614-627.e7

Hanzén S, Vielfort K, Yang J, Roger F, Andersson V, Zamarbide-Forés S, Andersson R, Malm L, Palais G, Biteau B, et al (2016) Lifespan Control by Redox-Dependent Recruitment of Chaperones to Misfolded Proteins. Cell **166**: 140–151

Hartl FU, Bracher A, Hayer-Hartl M (2011) Molecular chaperones in protein folding and proteostasis. Nature **475**: 324–332

Haunhorst P, Hanschmann E-M, Bräutigam L, Stehling O, Hoffmann B, Mühlenhoff U, Lill R, Berndt C, Lillig CH (2013) Crucial function of vertebrate glutaredoxin 3 (PICOT) in iron homeostasis and hemoglobin maturation. Mol Biol Cell **24**: 1895–1903

Hirata A, Klein BJ, Murakami KS (2008) The X-ray crystal structure of RNA polymerase from Archaea. Nature **451**: 851–854

Hooper CM, Castleden IR, Tanz SK, Aryamanesh N, Millar AH (2017) SUBA4: the interactive data analysis centre for Arabidopsis subcellular protein locations. Nucleic Acids Res **45**: D1064–D1074

Horowitz S, Koldewey P, Stull F, Bardwell JC (2018) Folding while bound to chaperones. Curr Opin Struct Biol **48**: 1–5

Hu Y, Wu Q, Peng Z, Sprague SA, Wang W, Park J, Akhunov E, Jagadish KSV, Nakata PA, Cheng N, et al (2017) Silencing of OsGRXS17 in rice improves drought stress tolerance by modulating ROS accumulation and stomatal closure. Sci Rep **7**: 15950

Huang J, Niazi AK, Young D, Rosado LA, Vertommen D, Bodra N, Abdelgawwad MR, Vignols F, Wei B, Wahni K, et al (2018) Self-protection of cytosolic malate dehydrogenase against oxidative stress in Arabidopsis. J Exp Bot **69**: 3491–3505

Iñigo S, Durand AN, Ritter A, Le Gall S, Termathe M, Klassen R, Tohge T, De Coninck B, Van Leene J, De Clercq R, et al (2016) Glutaredoxin GRXS17 Associates with the Cytosolic Iron-Sulfur Cluster Assembly Pathway. Plant Physiol **172**: 858–873

Jakob U, Eser M, Bardwell JC (2000) Redox switch of hsp33 has a novel zinc-binding motif. J Biol Chem **275**: 38302–38310

Jakob U, Muse W, Eser M, Bardwell JC (1999) Chaperone activity with a redox switch. Cell **96**: 341–352

Klinge S, Hirst J, Maman JD, Krude T, Pellegrini L (2007) An iron-sulfur domain of the eukaryotic primase is essential for RNA primer synthesis. Nat Struct Mol Biol **14**: 875–877

Knuesting J, Riondet C, Maria C, Kruse I, Bécuwe N, König N, Berndt C, Tourrette S, Guilleminot-Montoya J, Herrero E, et al (2015) Arabidopsis glutaredoxin S17 and its partner, the nuclear factor Y subunit C11/negative cofactor 2α, contribute to maintenance of the shoot apical meristem under long-day photoperiod. Plant Physiol **167**: 1643–1658

Koldewey P, Stull F, Horowitz S, Martin R, Bardwell JCA (2016) Forces Driving Chaperone Action. Cell **166**: 369–379

Lee JR, Lee SS, Jang HH, Lee YM, Park JH, Park S-C, Moon JC, Park SK, Kim SY, Lee SY, et al (2009) Heat-shock dependent oligomeric status alters the function of a plant-specific thioredoxin-like protein, AtTDX. Proc Natl Acad Sci U S A **106**: 5978–5983

Liebthal M, Maynard D, Dietz K-J (2018) Peroxiredoxins and Redox Signaling in Plants. Antioxid Redox Signal **28**: 609–624

Liedgens L, Zimmermann J, Wäschenbach L, Geissel F, Laporte H, Gohlke H, Morgan B, Deponte M (2020) Quantitative assessment of the determinant structural differences between redox-active and inactive glutaredoxins. Nat Commun **11**: 1725

Lill R (2009) Function and biogenesis of iron-sulphur proteins. Nature **460**: 831–838

Lillig CH, Berndt C, Vergnolle O, Lönn ME, Hudemann C, Bill E, Holmgren A (2005) Characterization of human glutaredoxin 2 as iron-sulfur protein: a possible role as redox sensor. Proc Natl Acad Sci U S A **102**: 8168–8173

Liu X, Liu S, Feng Y, Liu J-Z, Chen Y, Pham K, Deng H, Hirschi KD, Wang X, Cheng N (2013) Structural insights into the N-terminal GIY-YIG endonuclease activity of Arabidopsis glutaredoxin AtGRXS16 in chloroplasts. Proc Natl Acad Sci U S A **110**: 9565–9570

Mayer MP (2010) Gymnastics of molecular chaperones. Mol Cell **39**: 321–331

Meyer Y, Belin C, Delorme-Hinoux V, Reichheld J-P, Riondet C (2012) Thioredoxin and glutaredoxin systems in plants: molecular mechanisms, crosstalks, and functional significance. Antioxid Redox Signal **17**: 1124–1160

Meyer Y, Buchanan BB, Vignols F, Reichheld J-P (2009) Thioredoxins and glutaredoxins: unifying elements in redox biology. Annu Rev Genet **43**: 335–367

Micsonai A, Wien F, Kernya L, Lee Y-H, Goto Y, Réfrégiers M, Kardos J (2015) Accurate secondary structure prediction and fold recognition for circular dichroism spectroscopy. Proc Natl Acad Sci U S A **112**: E3095-3103

Molina MM, Bellí G, de la Torre MA, Rodríguez-Manzaneque MT, Herrero E (2004) Nuclear monothiol glutaredoxins of Saccharomyces cerevisiae can function as mitochondrial glutaredoxins. J Biol Chem **279**: 51923–51930

Moseler A, Aller I, Wagner S, Nietzel T, Przybyla-Toscano J, Mühlenhoff U, Lill R, Berndt C, Rouhier N, Schwarzländer M, et al (2015) The mitochondrial monothiol glutaredoxin S15 is essential for iron-sulfur protein maturation in Arabidopsis thaliana. Proc Natl Acad Sci U S A **112**: 13735–13740

Mühlenhoff U, Molik S, Godoy JR, Uzarska MA, Richter N, Seubert A, Zhang Y, Stubbe J, Pierrel F, Herrero E, et al (2010) Cytosolic monothiol glutaredoxins function in intracellular iron sensing and trafficking via their bound iron-sulfur cluster. Cell Metab **12**: 373–385

Mulekar JJ, Huq E (2014) Expanding roles of protein kinase CK2 in regulating plant growth and development. J Exp Bot **65**: 2883–2893

Park SK, Jung YJ, Lee JR, Lee YM, Jang HH, Lee SS, Park JH, Kim SY, Moon JC, Lee SY, et al (2009) Heat-shock and redox-dependent functional switching of an h-type Arabidopsis thioredoxin from a disulfide reductase to a molecular chaperone. Plant Physiol **150**: 552–561

Park S-W, Li W, Viehhauser A, He B, Kim S, Nilsson AK, Andersson MX, Kittle JD, Ambavaram MMR, Luan S, et al (2013) Cyclophilin 20-3 relays a 12-oxo-phytodienoic acid signal during stress responsive regulation of cellular redox homeostasis. Proc Natl Acad Sci U S A **110**: 9559–9564

Rey P, Becuwe N, Tourrette S, Rouhier N (2017) Involvement of Arabidopsis glutaredoxin S14 in the maintenance of chlorophyll content. Plant Cell Environ **40**: 2319–2332

Rey P, Taupin-Broggini M, Couturier J, Vignols F, Rouhier N (2019) Is There a Role for Glutaredoxins and BOLAs in the Perception of the Cellular Iron Status in Plants? Front Plant Sci **10**: 712

Riondet C, Desouris JP, Montoya JG, Chartier Y, Meyer Y, Reichheld J-P (2012) A dicotyledon-specific glutaredoxin GRXC1 family with dimer-dependent redox regulation is functionally redundant with GRXC2. Plant Cell Environ **35**: 360–373

Rouhier N, Lemaire SD, Jacquot J-P (2008) The role of glutathione in photosynthetic organisms: emerging functions for glutaredoxins and glutathionylation. Annu Rev Plant Biol **59**: 143–166

Rouhier N, Unno H, Bandyopadhyay S, Masip L, Kim S-K, Hirasawa M, Gualberto JM, Lattard V, Kusunoki M, Knaff DB, et al (2007) Functional, structural, and spectroscopic characterization of a glutathione-ligated [2Fe-2S] cluster in poplar glutaredoxin C1. Proc Natl Acad Sci U S A **104**: 7379–7384

Schwarzländer M, Fricker MD, Müller C, Marty L, Brach T, Novak J, Sweetlove LJ, Hell R, Meyer AJ (2008) Confocal imaging of glutathione redox potential in living plant cells. J Microsc **231**: 299–316

Ströher E, Grassl J, Carrie C, Fenske R, Whelan J, Millar AH (2016) Glutaredoxin S15 Is Involved in Fe-S Cluster Transfer in Mitochondria Influencing Lipoic Acid-Dependent Enzymes, Plant Growth, and Arsenic Tolerance in Arabidopsis. Plant Physiol **170**: 1284–1299

Stull F, Koldewey P, Humes JR, Radford SE, Bardwell JCA (2016) Substrate protein folds while it is bound to the ATP-independent chaperone Spy. Nat Struct Mol Biol **23**: 53–58

Truernit E, Haseloff J (2008) A simple way to identify non-viable cells within living plant tissue using confocal microscopy. Plant Methods **4**: 15

Trujillo-Hernandez JA, Bariat L, Enders TA, Strader LC, Reichheld J-P, Belin C (2020) A Glutathione-dependent control of IBA pathway supports Arabidopsis root system adaptation to phosphate deprivation. J Exp Bot. doi: 10.1093/jxb/eraa195

Voth W, Schick M, Gates S, Li S, Vilardi F, Gostimskaya I, Southworth DR, Schwappach B, Jakob U (2014) The protein targeting factor Get3 functions as ATP-independent chaperone under oxidative stress conditions. Mol Cell **56**: 116–127

Wang X, Chen X, Sun L, Qian W (2019) Canonical cytosolic iron-sulfur cluster assembly and non-canonical functions of DRE2 in Arabidopsis. PLoS Genet **15**: e1008094

Wang Y, Chang H, Hu S, Lu X, Yuan C, Zhang C, Wang P, Xiao W, Xiao L, Xue G-P, et al (2014) Plastid casein kinase 2 knockout reduces abscisic acid (ABA) sensitivity, thermotolerance, and expression of ABA- and heat-stress-responsive nuclear genes. J Exp Bot **65**: 4159–4175

Wingert RA, Galloway JL, Barut B, Foott H, Fraenkel P, Axe JL, Weber GJ, Dooley K, Davidson AJ, Schmid B, et al (2005) Deficiency of glutaredoxin 5 reveals Fe-S clusters are required for vertebrate haem synthesis. Nature **436**: 1035–1039

Winter J, Ilbert M, Graf PCF, Ozcelik D, Jakob U (2008) Bleach activates a redox-regulated chaperone by oxidative protein unfolding. Cell **135**: 691–701

Wu Q, Hu Y, Sprague SA, Kakeshpour T, Park J, Nakata PA, Cheng N, Hirschi KD, White FF, Park S (2017) Expression of a monothiol glutaredoxin, AtGRXS17, in tomato (Solanum lycopersicum) enhances drought tolerance. Biochem Biophys Res Commun **491**: 1034–1039

Wu Q, Lin J, Liu J-Z, Wang X, Lim W, Oh M, Park J, Rajashekar CB, Whitham SA, Cheng N-H, et al (2012) Ectopic expression of Arabidopsis glutaredoxin AtGRXS17 enhances thermotolerance in tomato. Plant Biotechnol J **10**: 945–955

Yan R, Adinolfi S, Iannuzzi C, Kelly G, Oregioni A, Martin S, Pastore A (2013) Cluster and Fold Stability of E. coli ISC-Type Ferredoxin. PLOS ONE **8**: e78948

Yeh C-H, Kaplinsky NJ, Hu C, Charng Y-Y (2012) Some like it hot, some like it warm: phenotyping to explore thermotolerance diversity. Plant Sci Int J Exp Plant Biol **195**: 10–23

Yu H, Yang J, Shi Y, Donelson J, Thompson SM, Sprague S, Roshan T, Wang D-L, Liu J, Park S, et al (2017) Arabidopsis Glutaredoxin S17 Contributes to Vegetative Growth, Mineral Accumulation, and Redox Balance during Iron Deficiency. Front Plant Sci **8**: 1045

Zaffagnini M, Michelet L, Massot V, Trost P, Lemaire SD (2008) Biochemical characterization of glutaredoxins from Chlamydomonas reinhardtii reveals the unique properties of a chloroplastic CGFS-type glutaredoxin. J Biol Chem **283**: 8868–8876

Zhang Y, Liu L, Wu X, An X, Stubbe J, Huang M (2011) Investigation of in vivo diferric tyrosyl radical formation in Saccharomyces cerevisiae Rnr2 protein: requirement of Rnr4 and contribution of Grx3/4 AND Dre2 proteins. J Biol Chem **286**: 41499–41509

Zhao C, Wang P, Si T, Hsu C-C, Wang L, Zayed O, Yu Z, Zhu Y, Dong J, Tao WA, et al (2017) MAP kinase cascades regulate the cold response by modulating ICE1 protein stability. Dev Cell **43**: 618-629.e5

892

893
894

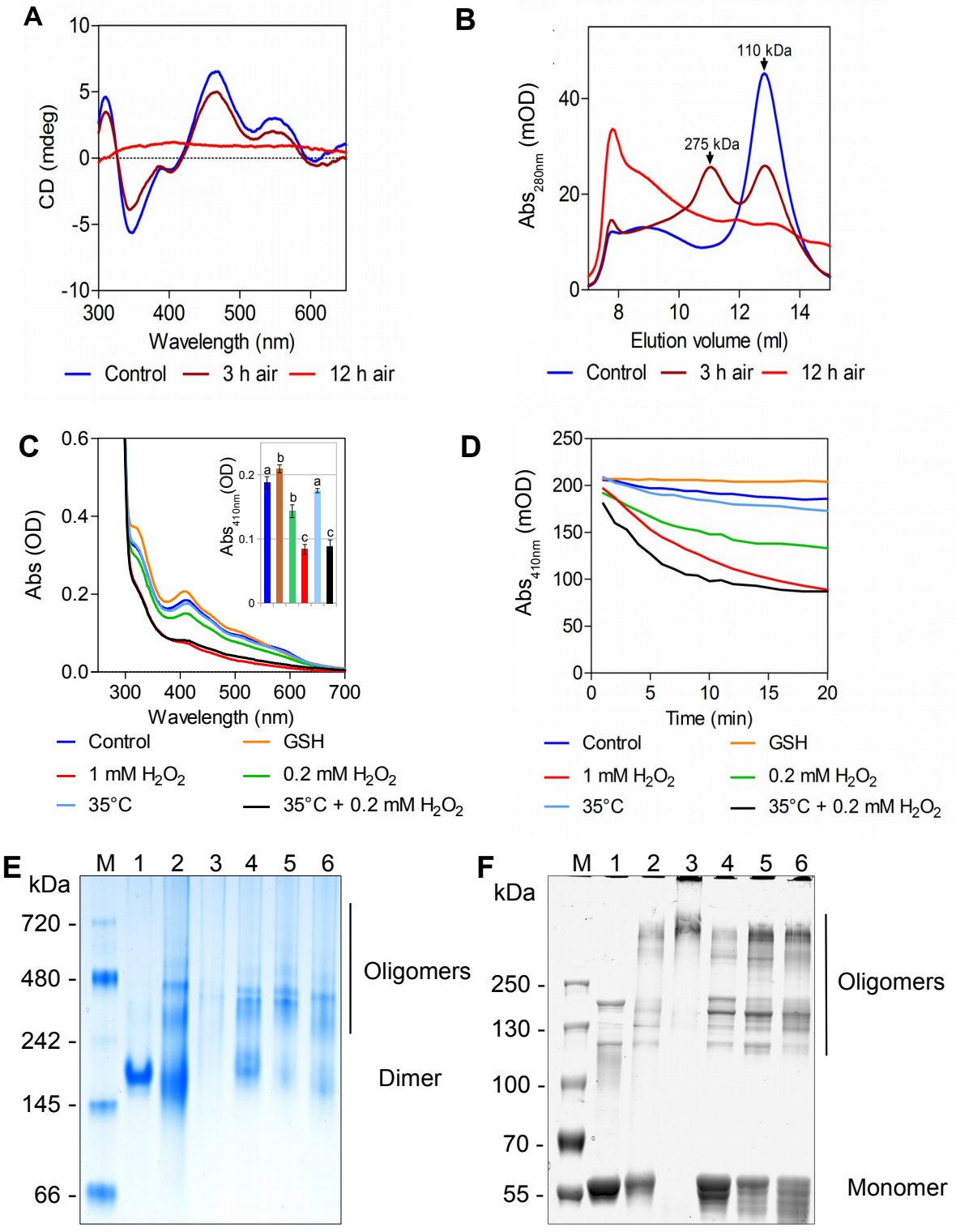

Figure 1: Fe-S cluster stability and oligomerization of reconstituted GRXS17. (A) Visible circular dichroism (CD)-spectra of reconstituted holo-GRXS17 under reducing conditions (blue) and after oxygen treatment (3h brown; 12h red) at room temperature. (B) Size-exclusion chromatography (Sephacryl S300 HR) under anaerobic conditions with reconstituted GRXS17 after the respective oxygen treatments. (C) Absorption spectra of GRXS17 subjected to H_2O_2 and heat treatments. UV-VIS absorption spectra were measured after *in vitro* reconstitution under anaerobic conditions and after 20 min of treatment with 20°C (blue), GSH at 20°C (2.5 mM orange), H_2O_2 at 20°C (0.2 mM green; 1 mM red), 35°C in presence of 0.2 mM H_2O_2 (black) or without H_2O_2 (light blue). Inset : Absorption at 410 nm of the same samples. Data are means of 3-6 biological repetitions +/- SE. The letters a, b and c indicate significance compared to the control (blue), of $p>0.1$, $p<0.001$, and $p<0.00001$, respectively, by Student's t-test. (D) Kinetics monitoring the GRXS17 Fe-S cluster stability subjected to the same treatments as in (C). (E-F) Migration of 5 µg of recombinant GRXS17 with or without the cluster in (E) native PAGE or (F) in non-reducing SDS-PAGE gels. M, Molecular marker. HoloGRXS17 (1) was maintained in air for 3h (2) or 12h (3) or treated for 10 min at 35°C (4), with 0.2 mM H_2O_2 (5) or a combination of both treatments (6). Samples were subjected to non-reducing SDS-PAGE and protein bands were stained by Coomassie blue. Each experiment is representative of three biological repetitions.

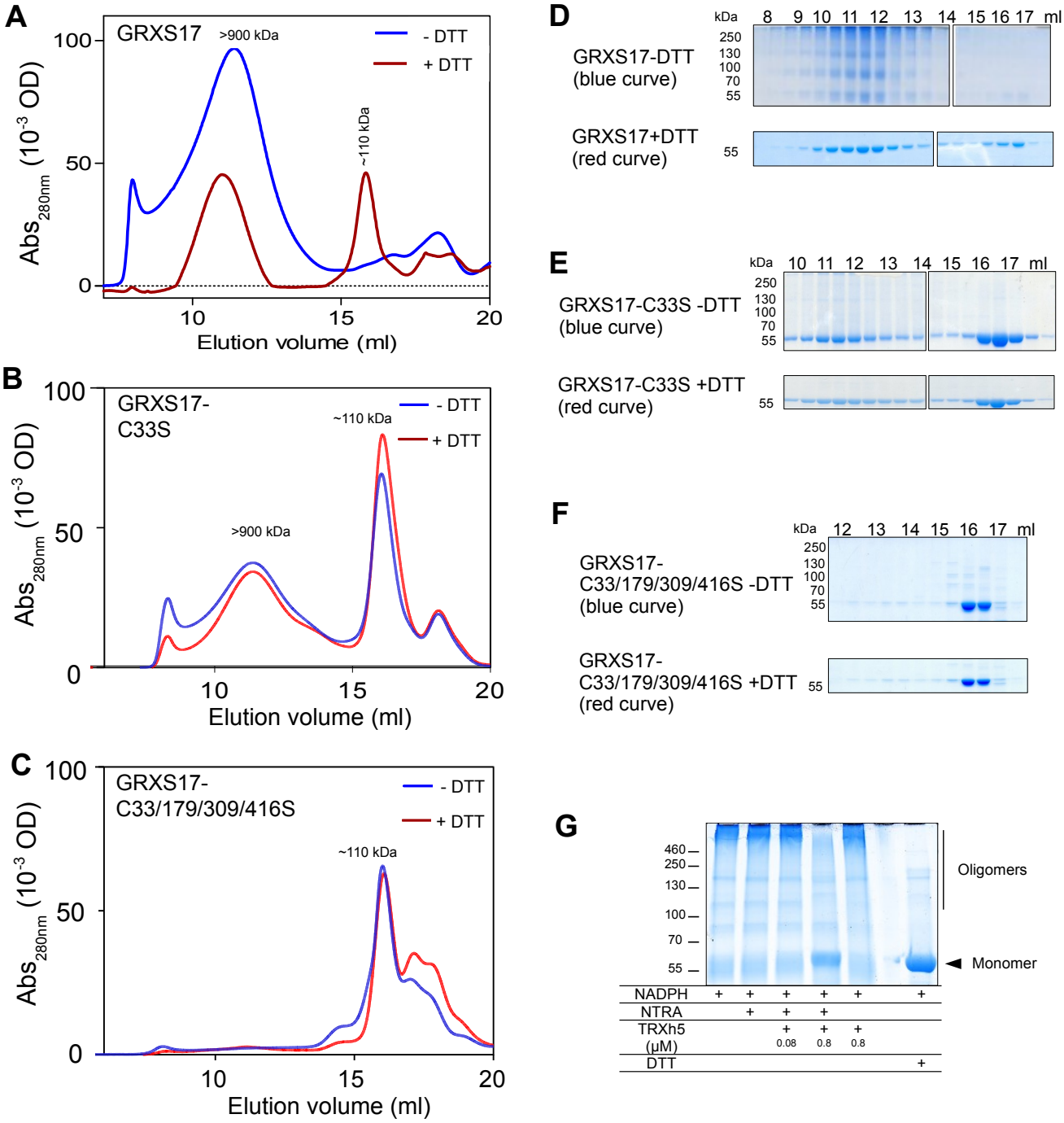

Figure 2: GRXS17 forms high molecular weight complexes.
(A,B,C) Size-exclusion chromatography (SEC) analysis (Superose 6) of 740 µg (A) GRXS17 protein, (B) GRXS17-C33S and (C) GRXS17-C33/179/309/416S maintained in air after purification. The protein was reduced with 100 mM DTT (red) or without (blue) before loading on the column. Approximative molecular weights were calculated based on the elution volume of reference proteins (see Methods). (D,E,F) Aliquots of elution fraction (30 µL) shown in (A,B,C) were subjected to non-reducing SDS-PAGE. (G) GRXS17 oligomers are reduced by the TRX system. Recombinant GRXS17 (5 µM) was incubated with NADPH (150 µM) for 1h at 30°C, with or without NTRA (0.8 µM), DTT (50 mM) and TRXh5 as indicated in the table. Afterwards, proteins were separated by non-reducing SDS-PAGE.

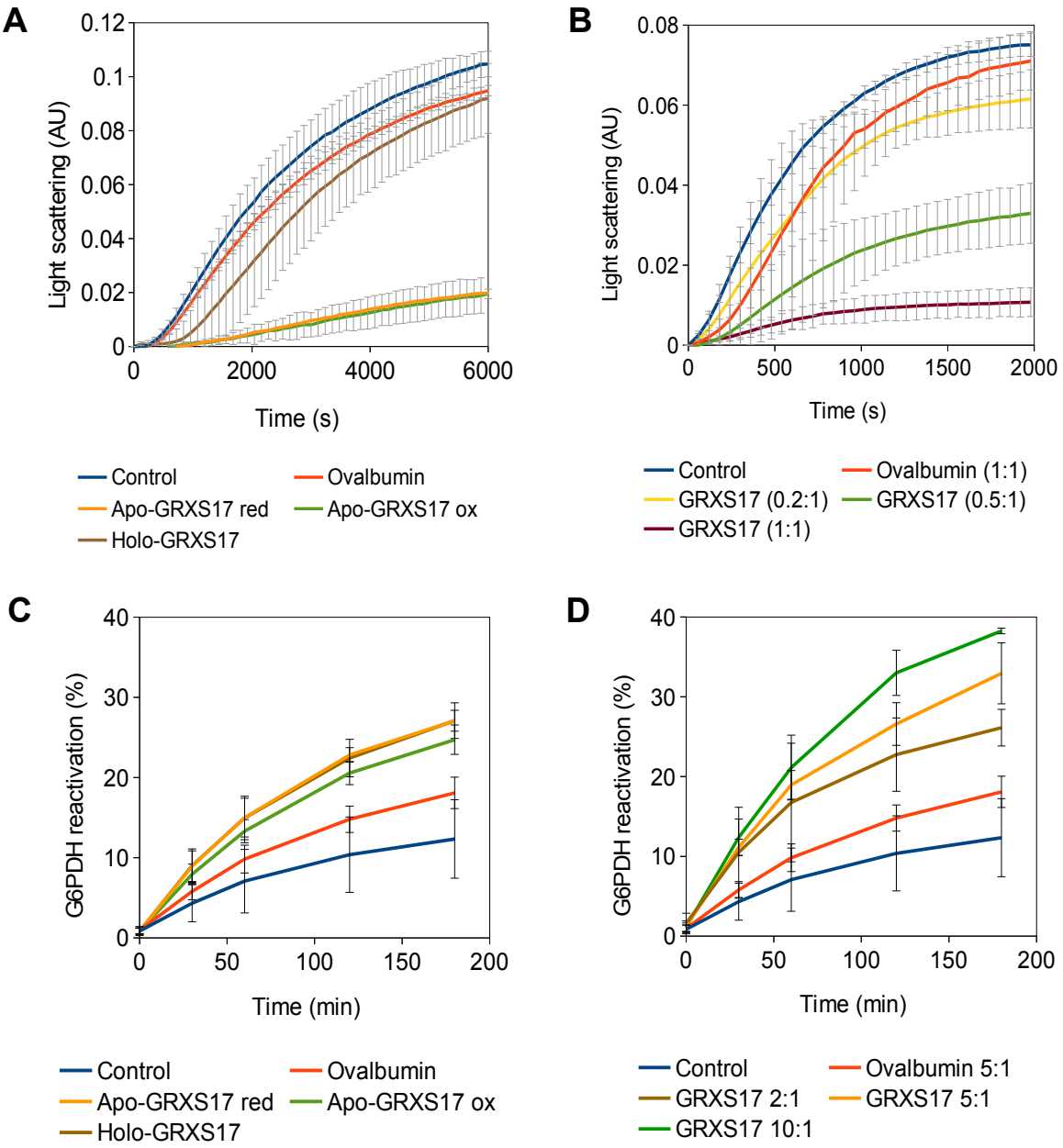

Figure 3: GRXS17 exhibits holdase and foldase chaperone activities.
(A-B) GRXS17 holdase activity toward citrate synthase (CS; A) or malate dehydrogenase (MDH; B) was measured by light scattering. CS or MDH were incubated alone (Control), with ovalbumin or with the different GRXS17 proteins. (A) Holo-GRXS17 or apo-GRXS17 in their reduced or oxidized forms were incubated with CS at a 1:1 (0.5:0.5 µM) ratio at 43°C. Ovalbumin ratios were 1:1 (0.5:0.5 µM). (B) Ratios of apo-GRXS17/MDH were 0.2:1 (0.1:0.5 µM), 0.5:1 (0.25:0.5 µM) and 1:1 (0.5:0.5 µM). Ovalbumin ratios were 1:1 (0.5:0.5 µM). (C-D) GRXS17 foldase activity was measured by reactivation of the glucose 6-phosphate dehydrogenase (G6PDH) activity after denaturation with urea. The zero time point represents the starting activity for the reactivation assay with 100% being the activity before heat denaturation. (C) Holo-GRXS17 or apo-GRXS17 in their reduced or oxidized forms were incubated with G6PDH at a 5:1 (0.65:0.13 µM) ratio at 30°C. Ovalbumin ratios were 5:1 (0.65:0.13 µM). D) Ratios of apo-GRXS17/G6PDH were 2:1 (0.26:0.13 µM), 5:1 (0.65:0.13 µM) and 10:1 (1.3:0.13 µM). Ovalbumin ratios were 5:1 (0.65:0.13 µM). Data are means of at least 3 biological repetitions +/- SE. Control and ovalbumin curves are the same and represent means and SD of all experiments (n>9).

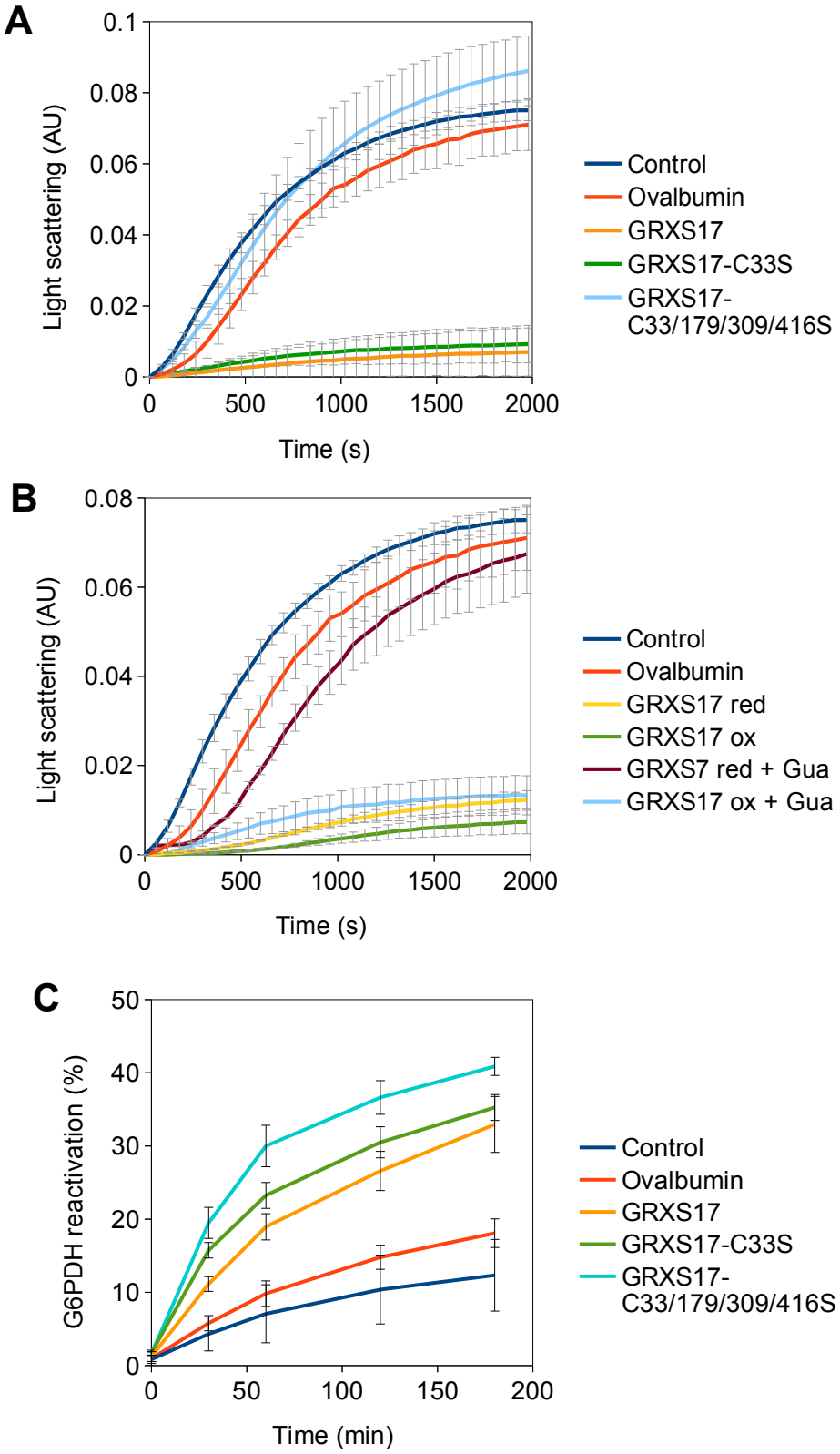

Figure 4: Role of GRXS17 active-site cysteines and oligomerization in holdase and foldase activities. (A) Holdase activity of GRXS17 and Cys-mutated GRXS17 proteins was measured toward MDH heat-induced precipitation by light scattering at 55°C. MDH was incubated alone (Control), with ovalbumin or with the different GRXS17 proteins at 1:1 (0.5:0.5 µM) ratios. (B) GRXS17 proteins reduced by 5 mM DTT (yellow) or oxidized with 1 mM H_2O_2 (green) were treated with 20 mM guanidinium hydrochloride (Gua) as a chaotropic reagent (brown and light blue, respectively). MDH was incubated alone (Control) or with ovalbumin. (C) Foldase activity of GRXS17 and Cys-mutated GRXS17 proteins was determined by measuring the glucose-6 phosphate dehydrogenase (G6PDH) activity after denaturation with urea. The zero time point represents the starting activity for the reactivation assay with 100% being the activity before heat denaturation. G6PDH was incubated alone (Control), with ovalbumin or with the different GRXS17 proteins at 5:1 (0.65:0.13 µM) ratios. Data are means of at least 3 biological repetitions +/- SE. Control and ovalbumin curves are the same and represent means and SD of all experiments made (n>9).

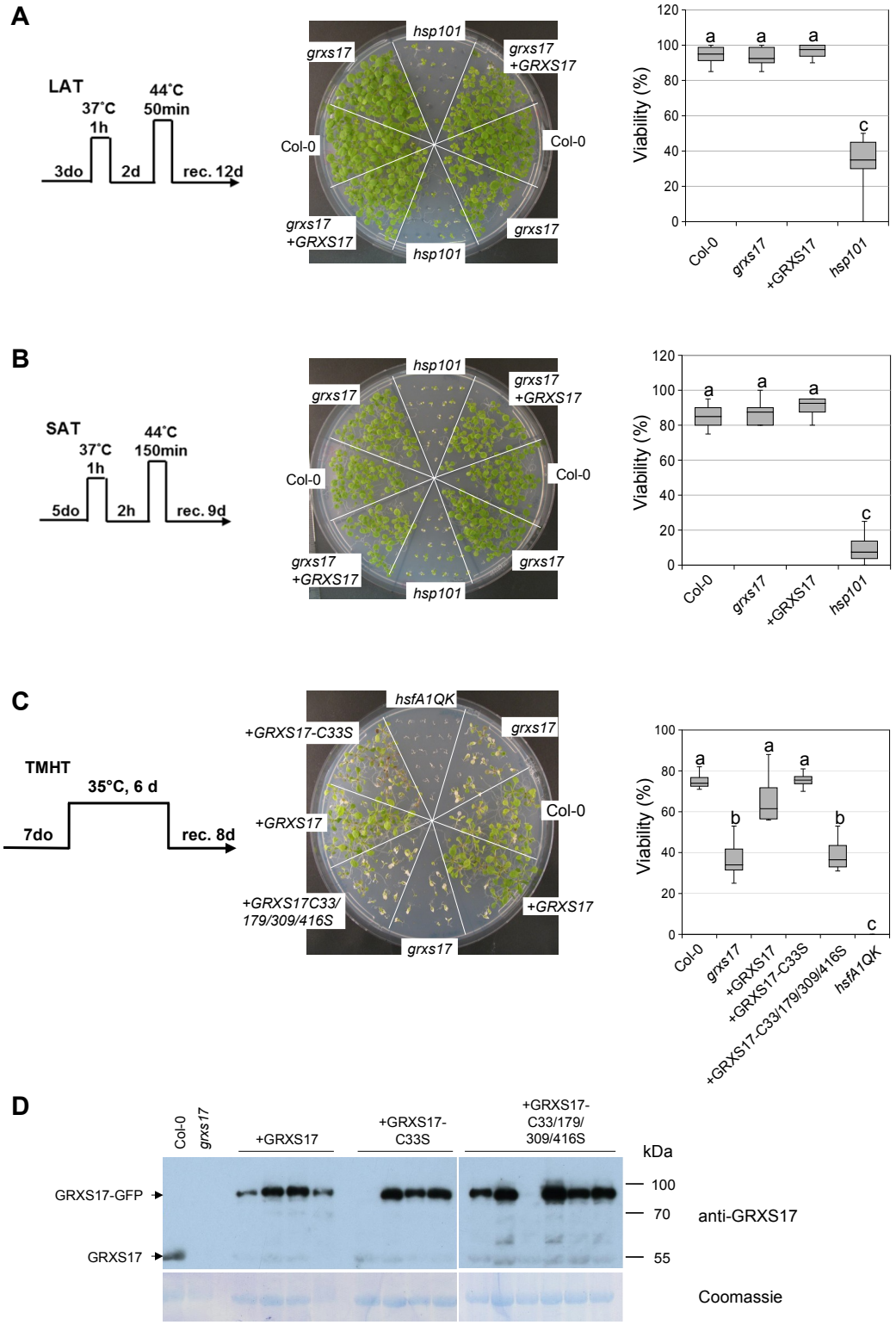

Figure 5: GRXS17 is specifically involved in thermotolerance to moderate high temperature. Wild-type plants (Col-0), the *grxs17* knock-out mutant (*grxs17*), the *grxs17* mutant complemented with a *Pr35S:GRXS17:GFP* construct expressing the GRXS17:GFP fusion protein (+GRXS17), the GRXS17-C33S:GFP protein (+GRXS17-C33S), the GRXS17-C33/179/309/416S:GFP (+GRXS17-C33/179/309/416S) protein, Heat-Shock Factor A1 quadruple knock-out mutant (*hsfA1QK*) or Heat-Shock Protein 101 knock-out mutant (*hsp101*) plants were subjected to different temperature stress regimes : (A) LAT, Long-term Acquired Thermotolerance ; (B) SAT, Short-term Acquired Thermotolerance ; (C) Thermotolerance to Moderate High Temperature (TMHT). do: days old. rec: recovery. Viability of the plants was assessed by recovery of shoot growth. Data are means of 4-10 biological repetitions +/- SE, n = 20-25. The letters a, b and c indicate a significance compared to Col-0, of $p>0.1$, $p<0.001$, and $p<0.00001$, respectively, by Student's t-test. (D) GRXS17 protein expression in complemented *grxs17* lines. Total protein extracts were prepared from 2-week-old plantlets. Protein extracts were separated by SDS-PAGE and probed with antibodies directed against GRXS17. Plants expressing the transgenes at different levels are represented. In Col-0, the 50 kDa signal corresponds to the native GRXS17 protein. In the complemented lines, the 80 kDa signal corresponds to the GRXS17:GFP fusion protein.

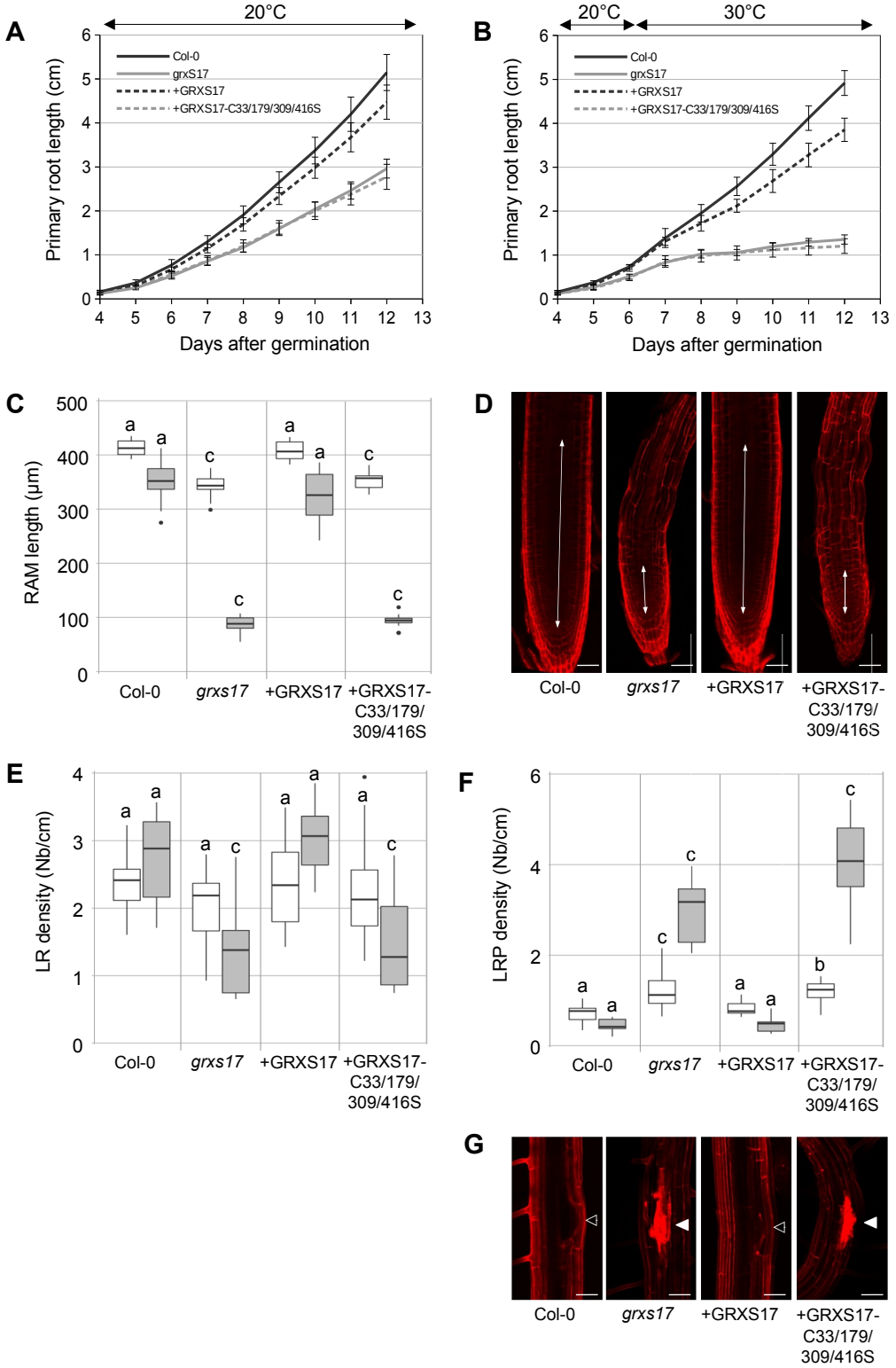

Figure 6: GRXS17 is involved in root development under heat stress. Wild-type (Col-0), the *grxs17* knock-out mutant (*grxs17*), the *grxs17* mutant complemented with a *Pr35S:GRXS17:GFP* construct (+GRXS17) and the *Pr35S:GRXS17-C33/179/309/416S:GFP* construct (+GRXS17-C33/179/309/416S) plants were grown 12 days continuously at 20°C or 6 days at 20°C and shifted to 30°C for 6 more days. (A-B) Primary root length of plants grown at 20°C (A) or shifted to 30°C (B). (C) Root apical meristem (RAM) of plants grown at 20°C (white boxplots) or shifted to 30°C (grey boxplots). (D) RAM of plants shifted to 30°C and stained by propidium iodide. RAM length (bidirectional arrows) was determined by the distance from the quiescent center to where endodermis cells were elongating. (E-F) Density (number per cm of primary root) of emerged lateral roots (LR; E) and lateral root primordia (LRP) after growth at 20°C (white boxplots) or shifted to 30°C (grey boxplots). (G) LRP of plants shifted to30°C and stained by propidium iodide. White arrowheads pinpoint cell death in LRP, whereas unfilled arrowheads represent LRP where cell death did not occur. Data are means of 3 biological repetitions +/- SE, n = 15. The letters a, b and c indicate a significance compared to Col-0, of $p>0.1$, $p<0.001$, and $p<0.00001$ respectively, by Student's t-test.

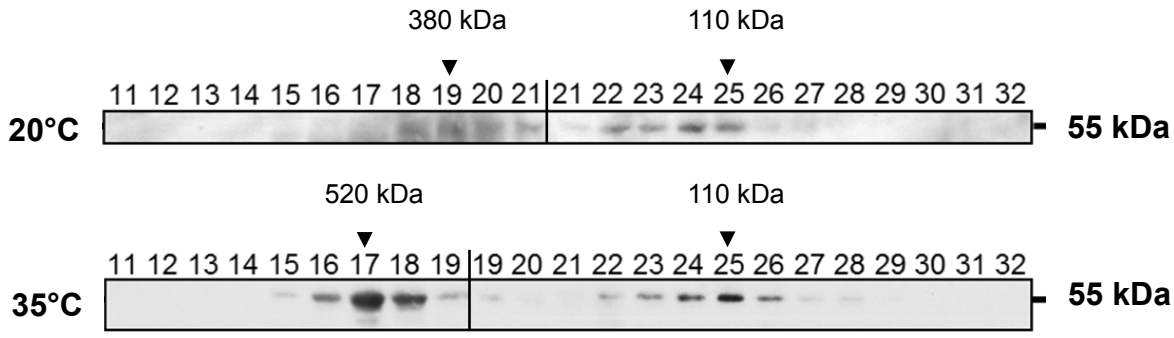

Figure 7: GRXS17 forms high molecular weight complexes in plant extracts. Size-exclusion chromatography analysis (Sephacryl S300 HR) of crude protein extracts from Arabidopsis seedlings cultivated 14 days at 20°C and further treated for 2 h at 35°C. The GRXS17 protein was detected after immunoblotting and immunodetection using an anti-GRXS17 serum. Numbered lines correspond to the protein fractions. Protein size of the respective fractions was obtained after calibration using marker proteins.

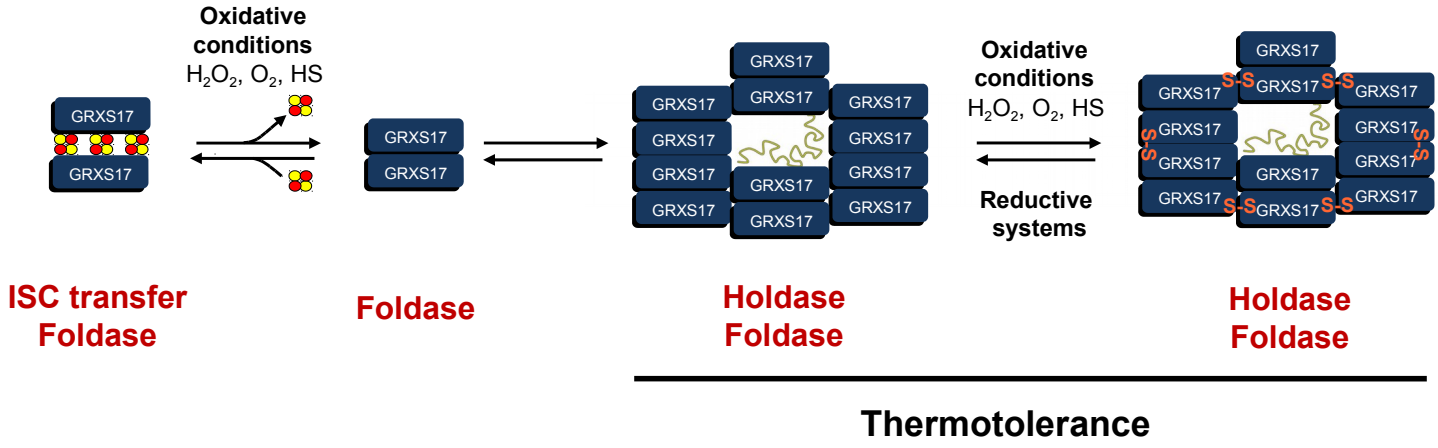

Figure 8: Model of the GRXS17-redox switch. Under reducing conditions, the holo-GRXS17 forms a dimer which coordinates an iron-sulfur cluster (ISC). In this form, GRXS17 can transfer ISC to cytosolic or nuclear target proteins (represented as a green line in the middle of the oligomeric structures). Under oxidative conditions (H_2O_2, O_2, Heat Stress (HS)), ISC are released and GRXS17 switches to an apo-dimeric form with a foldase activity. Dimers can spontaneously associate to oligomeric forms and further oxidation induces oligomeric structure through formation of intermolecular disulfide bonds at active-site Cys residues. In this form, GRXS17 acquires holdase activities and provides thermotolerance. The oligomeric form can be reduced to recover the apo-dimeric GRXS17 and the Fe-S cluster can eventually be reassembled.

Parsed Citations

Ali Khan H, Mutus B (2014) Protein disulfide isomerase a multifunctional protein with multiple physiological roles. Front Chem 2: 70
Pubmed: Author and Title
Google Scholar: Author Only Title Only Author and Title

Banci L, Ciofi-Baffoni S, Gajda K, Muzzioli R, Peruzzini R, Winkelmann J (2015) N-terminal domains mediate [2Fe-2S] cluster transfer from glutaredoxin-3 to anamorsin. Nat Chem Biol 11: 772–778
Pubmed: Author and Title
Google Scholar: Author Only Title Only Author and Title

Bandyopadhyay S, Gama F, Molina-Navarro MM, Gualberto JM, Claxton R, Naik SG, Huynh BH, Herrero E, Jacquot JP, Johnson MK, et al (2008) Chloroplast monothiol glutaredoxins as scaffold proteins for the assembly and delivery of [2Fe-2S] clusters. EMBO J 27: 1122–1133
Pubmed: Author and Title
Google Scholar: Author Only Title Only Author and Title

Begas P, Liedgens L, Moseler A, Meyer AJ, Deponte M (2017) Glutaredoxin catalysis requires two distinct glutathione interaction sites. Nat Commun 8: 14835
Pubmed: Author and Title
Google Scholar: Author Only Title Only Author and Title

Berndt C, Hudemann C, Hanschmann E-M, Axelsson R, Holmgren A, Lillig CH (2007) How does iron-sulfur cluster coordination regulate the activity of human glutaredoxin 2? Antioxid Redox Signal 9: 151–157

Berndt C, Lillig CH (2017) Glutathione, Glutaredoxins, and Iron. Antioxid Redox Signal 27: 1235–1251
Pubmed: Author and Title
Google Scholar: Author Only Title Only Author and Title

Chae HB, Moon JC, Shin MR, Chi YH, Jung YJ, Lee SY, Nawkar GM, Jung HS, Hyun JK, Kim WY, et al (2013) Thioredoxin reductase type C (NTRC) orchestrates enhanced thermotolerance to Arabidopsis by its redox-dependent holdase chaperone function. Mol Plant 6: 323–336
Pubmed: Author and Title
Google Scholar: Author Only Title Only Author and Title

Cheng N-H, Liu J-Z, Liu X, Wu Q, Thompson SM, Lin J, Chang J, Whitham SA, Park S, Cohen JD, et al (2011) Arabidopsis monothiol glutaredoxin, AtGRXS17, is critical for temperature-dependent postembryonic growth and development via modulating auxin response. J Biol Chem 286: 20398–20406
Pubmed: Author and Title
Google Scholar: Author Only Title Only Author and Title

Choudhury FK, Rivero RM, Blumwald E, Mittler R (2017) Reactive oxygen species, abiotic stress and stress combination. Plant J 90: 856–867
Pubmed: Author and Title
Google Scholar: Author Only Title Only Author and Title

Clough SJ, Bent AF (1998) Floral dip: a simplified method for Agrobacterium-mediated transformation of Arabidopsis thaliana. Plant J Cell Mol Biol 16: 735–743
Pubmed: Author and Title
Google Scholar: Author Only Title Only Author and Title

Couturier J, Jacquot J-P, Rouhier N (2009) Evolution and diversity of glutaredoxins in photosynthetic organisms. Cell Mol Life Sci CMLS 66: 2539–2557
Pubmed: Author and Title
Google Scholar: Author Only Title Only Author and Title

Couturier J, Przybyla-Toscano J, Roret T, Didierjean C, Rouhier N (2015) The roles of glutaredoxins ligating Fe-S clusters: Sensing, transfer or repair functions? Biochim Biophys Acta 1853: 1513–1527

Couturier J, Ströher E, Albetel A-N, Roret T, Muthuramalingam M, Tarrago L, Seidel T, Tsan P, Jacquot J-P, Johnson MK, et al (2011) Arabidopsis chloroplastic glutaredoxin C5 as a model to explore molecular determinants for iron-sulfur cluster binding into glutaredoxins. J Biol Chem 286: 27515–27527
Pubmed: Author and Title
Google Scholar: Author Only Title Only Author and Title

Couturier J, Touraine B, Briat J-F, Gaymard F, Rouhier N (2013) The iron-sulfur cluster assembly machineries in plants: current knowledge and open questions. Front Plant Sci 4: 259
Pubmed: Author and Title
Google Scholar: Author Only Title Only Author and Title

Couturier J, Wu H-C, Dhalleine T, Pégeot H, Sudre D, Gualberto JM, Jacquot J-P, Gaymard F, Vignols F, Rouhier N (2014) Monothiol glutaredoxin-BolA interactions: redox control of Arabidopsis thaliana BolA2 and SufE1. Mol Plant 7: 187–205
Pubmed: Author and Title
Google Scholar: Author Only Title Only Author and Title

Dickinson PJ, Kumar M, Martinho C, Yoo SJ, Lan H, Artavanis G, Charoensawan V, Schöttler MA, Bock R, Jaeger KE, et al (2018) Chloroplast Signaling Gates Thermotolerance in Arabidopsis. Cell Rep 22: 1657–1665
Pubmed: Author and Title
Google Scholar: Author Only Title Only Author and Title

Encinar del Dedo J, Gabrielli N, Carmona M, Ayté J, Hidalgo E (2015) A cascade of iron-containing proteins governs the genetic iron starvation response to promote iron uptake and inhibit iron storage in fission yeast. PLoS Genet 11: e1005106
Pubmed: Author and Title
Google Scholar: Author Only Title Only Author and Title

Frey AG, Palenchar DJ, Wildemann JD, Philpott CC (2016) A Glutaredoxin·BolA Complex Serves as an Iron-Sulfur Cluster Chaperone for the Cytosolic Cluster Assembly Machinery. J Biol Chem 291: 22344–22356
Pubmed: Author and Title
Google Scholar: Author Only Title Only Author and Title

Goemans CV, Vertommen D, Agrebi R, Collet J-F (2018) CnoX Is a Chaperedoxin: A Holdase that Protects Its Substrates from Irreversible Oxidation. Mol Cell 70: 614-627.e7
Pubmed: Author and Title
Google Scholar: Author Only Title Only Author and Title

Hanzén S, Vielfort K, Yang J, Roger F, Andersson V, Zamarbide-Forés S, Andersson R, Malm L, Palais G, Biteau B, et al (2016) Lifespan Control by Redox-Dependent Recruitment of Chaperones to Misfolded Proteins. Cell 166: 140–151
Pubmed: Author and Title
Google Scholar: Author Only Title Only Author and Title

Hartl FU, Bracher A, Hayer-Hartl M (2011) Molecular chaperones in protein folding and proteostasis. Nature 475: 324–332
Pubmed: Author and Title
Google Scholar: Author Only Title Only Author and Title

Haunhorst P, Hanschmann E-M, Bräutigam L, Stehling O, Hoffmann B, Mühlenhoff U, Lill R, Berndt C, Lillig CH (2013) Crucial function of vertebrate glutaredoxin 3 (PICOT) in iron homeostasis and hemoglobin maturation. Mol Biol Cell 24: 1895–1903
Pubmed: Author and Title
Google Scholar: Author Only Title Only Author and Title

Hirata A, Klein BJ, Murakami KS (2008) The X-ray crystal structure of RNA polymerase from Archaea. Nature 451: 851–854
Pubmed: Author and Title
Google Scholar: Author Only Title Only Author and Title

Hooper CM, Castleden IR, Tanz SK, Aryamanesh N, Millar AH (2017) SUBA4: the interactive data analysis centre for Arabidopsis subcellular protein locations. Nucleic Acids Res 45: D1064–D1074
Pubmed: Author and Title
Google Scholar: Author Only Title Only Author and Title

Horowitz S, Koldewey P, Stull F, Bardwell JC (2018) Folding while bound to chaperones. Curr Opin Struct Biol 48: 1–5
Pubmed: Author and Title
Google Scholar: Author Only Title Only Author and Title

Hu Y, Wu Q, Peng Z, Sprague SA, Wang W, Park J, Akhunov E, Jagadish KSV, Nakata PA, Cheng N, et al (2017) Silencing of OsGRXS17 in rice improves drought stress tolerance by modulating ROS accumulation and stomatal closure. Sci Rep 7: 15950
Pubmed: Author and Title
Google Scholar: Author Only Title Only Author and Title

Huang J, Niazi AK, Young D, Rosado LA, Vertommen D, Bodra N, Abdelgawwad MR, Vignols F, Wei B, Wahni K, et al (2018) Self-protection of cytosolic malate dehydrogenase against oxidative stress in Arabidopsis. J Exp Bot 69: 3491–3505
Pubmed: Author and Title
Google Scholar: Author Only Title Only Author and Title

Iñigo S, Durand AN, Ritter A, Le Gall S, Termathe M, Klassen R, Tohge T, De Coninck B, Van Leene J, De Clercq R, et al (2016) Glutaredoxin GRXS17 Associates with the Cytosolic Iron-Sulfur Cluster Assembly Pathway. Plant Physiol 172: 858–873
Pubmed: Author and Title
Google Scholar: Author Only Title Only Author and Title

Jakob U, Eser M, Bardwell JC (2000) Redox switch of hsp33 has a novel zinc-binding motif. J Biol Chem 275: 38302–38310
Pubmed: Author and Title
Google Scholar: Author Only Title Only Author and Title

Jakob U, Muse W, Eser M, Bardwell JC (1999) Chaperone activity with a redox switch. Cell 96: 341–352
Pubmed: Author and Title
Google Scholar: Author Only Title Only Author and Title

Klinge S, Hirst J, Maman JD, Krude T, Pellegrini L (2007) An iron-sulfur domain of the eukaryotic primase is essential for RNA primer synthesis. Nat Struct Mol Biol 14: 875–877
Pubmed: Author and Title
Google Scholar: Author Only Title Only Author and Title

Knuesting J, Riondet C, Maria C, Kruse I, Bécuwe N, König N, Berndt C, Tourrette S, Guilleminot-Montoya J, Herrero E, et al (2015) Arabidopsis glutaredoxin S17 and its partner, the nuclear factor Y subunit C11/negative cofactor 2α, contribute to maintenance of the shoot apical meristem under long-day photoperiod. Plant Physiol 167: 1643–1658
Pubmed: Author and Title
Google Scholar: Author Only Title Only Author and Title

Koldewey P, Stull F, Horowitz S, Martin R, Bardwell JCA (2016) Forces Driving Chaperone Action. Cell 166: 369–379
Pubmed: Author and Title
Google Scholar: Author Only Title Only Author and Title

Lee JR, Lee SS, Jang HH, Lee YM, Park JH, Park S-C, Moon JC, Park SK, Kim SY, Lee SY, et al (2009) Heat-shock dependent oligomeric status alters the function of a plant-specific thioredoxin-like protein, AtTDX. Proc Natl Acad Sci U S A 106: 5978–5983
Pubmed: Author and Title
Google Scholar: Author Only Title Only Author and Title

Liebthal M, Maynard D, Dietz K-J (2018) Peroxiredoxins and Redox Signaling in Plants. Antioxid Redox Signal 28: 609–624
Pubmed: Author and Title
Google Scholar: Author Only Title Only Author and Title

Liedgens L, Zimmermann J, Wäschenbach L, Geissel F, Laporte H, Gohlke H, Morgan B, Deponte M (2020) Quantitative assessment of the determinant structural differences between redox-active and inactive glutaredoxins. Nat Commun 11: 1725
Pubmed: Author and Title
Google Scholar: Author Only Title Only Author and Title

Lill R (2009) Function and biogenesis of iron-sulphur proteins. Nature 460: 831–838
Pubmed: Author and Title
Google Scholar: Author Only Title Only Author and Title

Lillig CH, Berndt C, Vergnolle O, Lönn ME, Hudemann C, Bill E, Holmgren A (2005) Characterization of human glutaredoxin 2 as iron-sulfur protein: a possible role as redox sensor. Proc Natl Acad Sci U S A 102: 8168–8173
Pubmed: Author and Title
Google Scholar: Author Only Title Only Author and Title

Liu X, Liu S, Feng Y, Liu J-Z, Chen Y, Pham K, Deng H, Hirschi KD, Wang X, Cheng N (2013) Structural insights into the N-terminal GIY-YIG endonuclease activity of Arabidopsis glutaredoxin AtGRXS16 in chloroplasts. Proc Natl Acad Sci U S A 110: 9565–9570
Pubmed: Author and Title
Google Scholar: Author Only Title Only Author and Title

Mayer MP (2010) Gymnastics of molecular chaperones. Mol Cell 39: 321–331
Pubmed: Author and Title
Google Scholar: Author Only Title Only Author and Title

Meyer Y, Belin C, Delorme-Hinoux V, Reichheld J-P, Riondet C (2012) Thioredoxin and glutaredoxin systems in plants: molecular mechanisms, crosstalks, and functional significance. Antioxid Redox Signal 17: 1124–1160
Pubmed: Author and Title
Google Scholar: Author Only Title Only Author and Title

Meyer Y, Buchanan BB, Vignols F, Reichheld J-P (2009) Thioredoxins and glutaredoxins: unifying elements in redox biology. Annu Rev Genet 43: 335–367
Pubmed: Author and Title
Google Scholar: Author Only Title Only Author and Title

Micsonai A, Wien F, Kernya L, Lee Y-H, Goto Y, Réfrégiers M, Kardos J (2015) Accurate secondary structure prediction and fold recognition for circular dichroism spectroscopy. Proc Natl Acad Sci U S A 112: E3095-3103
Pubmed: Author and Title
Google Scholar: Author Only Title Only Author and Title

Molina MM, Bellí G, de la Torre MA, Rodríguez-Manzaneque MT, Herrero E (2004) Nuclear monothiol glutaredoxins of Saccharomyces cerevisiae can function as mitochondrial glutaredoxins. J Biol Chem 279: 51923–51930
Pubmed: Author and Title
Google Scholar: Author Only Title Only Author and Title

Moseler A, Aller I, Wagner S, Nietzel T, Przybyla-Toscano J, Mühlenhoff U, Lill R, Berndt C, Rouhier N, Schwarzländer M, et al (2015) The mitochondrial monothiol glutaredoxin S15 is essential for iron-sulfur protein maturation in Arabidopsis thaliana. Proc Natl Acad Sci U S A 112: 13735–13740
Pubmed: Author and Title
Google Scholar: Author Only Title Only Author and Title

Mühlenhoff U, Molik S, Godoy JR, Uzarska MA, Richter N, Seubert A, Zhang Y, Stubbe J, Pierrel F, Herrero E, et al (2010) Cytosolic monothiol glutaredoxins function in intracellular iron sensing and trafficking via their bound iron-sulfur cluster. Cell Metab 12: 373–385
Pubmed: Author and Title
Google Scholar: Author Only Title Only Author and Title

Mulekar JJ, Huq E (2014) Expanding roles of protein kinase CK2 in regulating plant growth and development. J Exp Bot 65: 2883–2893

Pubmed: Author and Title
Google Scholar: Author Only Title Only Author and Title

Park SK, Jung YJ, Lee JR, Lee YM, Jang HH, Lee SS, Park JH, Kim SY, Moon JC, Lee SY, et al (2009) Heat-shock and redox-dependent functional switching of an h-type Arabidopsis thioredoxin from a disulfide reductase to a molecular chaperone. Plant Physiol 150: 552–561

Pubmed: Author and Title
Google Scholar: Author Only Title Only Author and Title

Park S-W, Li W, Viehhauser A, He B, Kim S, Nilsson AK, Andersson MX, Kittle JD, Ambavaram MMR, Luan S, et al (2013) Cyclophilin 20-3 relays a 12-oxo-phytodienoic acid signal during stress responsive regulation of cellular redox homeostasis. Proc Natl Acad Sci U S A 110: 9559–9564

Pubmed: Author and Title
Google Scholar: Author Only Title Only Author and Title

Rey P, Becuwe N, Tourrette S, Rouhier N (2017) Involvement of Arabidopsis glutaredoxin S14 in the maintenance of chlorophyll content. Plant Cell Environ 40: 2319–2332

Pubmed: Author and Title
Google Scholar: Author Only Title Only Author and Title

Rey P, Taupin-Broggini M, Couturier J, Vignols F, Rouhier N (2019) Is There a Role for Glutaredoxins and BOLAs in the Perception of the Cellular Iron Status in Plants? Front Plant Sci 10: 712

Riondet C, Desouris JP, Montoya JG, Chartier Y, Meyer Y, Reichheld J-P (2012) A dicotyledon-specific glutaredoxin GRXC1 family with dimer-dependent redox regulation is functionally redundant with GRXC2. Plant Cell Environ 35: 360–373

Pubmed: Author and Title
Google Scholar: Author Only Title Only Author and Title

Rouhier N, Lemaire SD, Jacquot J-P (2008) The role of glutathione in photosynthetic organisms: emerging functions for glutaredoxins and glutathionylation. Annu Rev Plant Biol 59: 143–166

Pubmed: Author and Title
Google Scholar: Author Only Title Only Author and Title

Rouhier N, Unno H, Bandyopadhyay S, Masip L, Kim S-K, Hirasawa M, Gualberto JM, Lattard V, Kusunoki M, Knaff DB, et al (2007) Functional, structural, and spectroscopic characterization of a glutathione-ligated [2Fe-2S] cluster in poplar glutaredoxin C1. Proc Natl Acad Sci U S A 104: 7379–7384

Pubmed: Author and Title
Google Scholar: Author Only Title Only Author and Title

Schwarzländer M, Fricker MD, Müller C, Marty L, Brach T, Novak J, Sweetlove LJ, Hell R, Meyer AJ (2008) Confocal imaging of glutathione redox potential in living plant cells. J Microsc 231: 299–316

Pubmed: Author and Title
Google Scholar: Author Only Title Only Author and Title

Ströher E, Grassl J, Carrie C, Fenske R, Whelan J, Millar AH (2016) Glutaredoxin S15 Is Involved in Fe-S Cluster Transfer in Mitochondria Influencing Lipoic Acid-Dependent Enzymes, Plant Growth, and Arsenic Tolerance in Arabidopsis. Plant Physiol 170: 1284–1299

Pubmed: Author and Title
Google Scholar: Author Only Title Only Author and Title

Stull F, Koldewey P, Humes JR, Radford SE, Bardwell JCA (2016) Substrate protein folds while it is bound to the ATP-independent chaperone Spy. Nat Struct Mol Biol 23: 53–58

Pubmed: Author and Title
Google Scholar: Author Only Title Only Author and Title

Truernit E, Haseloff J (2008) A simple way to identify non-viable cells within living plant tissue using confocal microscopy. Plant Methods 4: 15

Pubmed: Author and Title
Google Scholar: Author Only Title Only Author and Title

Trujillo-Hernandez JA, Bariat L, Enders TA, Strader LC, Reichheld J-P, Belin C (2020) A Glutathione-dependent control of IBA pathway supports Arabidopsis root system adaptation to phosphate deprivation. J Exp Bot. doi: 10.1093/jxb/eraa195

Pubmed: Author and Title
Google Scholar: Author Only Title Only Author and Title

Voth W, Schick M, Gates S, Li S, Vilardi F, Gostimskaya I, Southworth DR, Schwappach B, Jakob U (2014) The protein targeting factor Get3 functions as ATP-independent chaperone under oxidative stress conditions. Mol Cell 56: 116–127

Pubmed: Author and Title
Google Scholar: Author Only Title Only Author and Title

Wang X, Chen X, Sun L, Qian W (2019) Canonical cytosolic iron-sulfur cluster assembly and non-canonical functions of DRE2 in Arabidopsis. PLoS Genet 15: e1008094

Pubmed: Author and Title
Google Scholar: Author Only Title Only Author and Title

Wang Y, Chang H, Hu S, Lu X, Yuan C, Zhang C, Wang P, Xiao W, Xiao L, Xue G-P, et al (2014) Plastid casein kinase 2 knockout reduces abscisic acid (ABA) sensitivity, thermotolerance, and expression of ABA- and heat-stress-responsive nuclear genes. J Exp Bot 65: 4159–4175
Pubmed: Author and Title
Google Scholar: Author Only Title Only Author and Title

Wingert RA, Galloway JL, Barut B, Foott H, Fraenkel P, Axe JL, Weber GJ, Dooley K, Davidson AJ, Schmid B, et al (2005) Deficiency of glutaredoxin 5 reveals Fe-S clusters are required for vertebrate haem synthesis. Nature 436: 1035–1039
Pubmed: Author and Title
Google Scholar: Author Only Title Only Author and Title

Winter J, Ilbert M, Graf PCF, Ozcelik D, Jakob U (2008) Bleach activates a redox-regulated chaperone by oxidative protein unfolding. Cell 135: 691–701
Pubmed: Author and Title
Google Scholar: Author Only Title Only Author and Title

Wu Q, Hu Y, Sprague SA, Kakeshpour T, Park J, Nakata PA, Cheng N, Hirschi KD, White FF, Park S (2017) Expression of a monothiol glutaredoxin, AtGRXS17, in tomato (Solanum lycopersicum) enhances drought tolerance. Biochem Biophys Res Commun 491: 1034–1039
Pubmed: Author and Title
Google Scholar: Author Only Title Only Author and Title

Wu Q, Lin J, Liu J-Z, Wang X, Lim W, Oh M, Park J, Rajashekar CB, Whitham SA, Cheng N-H, et al (2012) Ectopic expression of Arabidopsis glutaredoxin AtGRXS17 enhances thermotolerance in tomato. Plant Biotechnol J 10: 945–955
Pubmed: Author and Title
Google Scholar: Author Only Title Only Author and Title

Yan R, Adinolfi S, Iannuzzi C, Kelly G, Oregioni A, Martin S, Pastore A (2013) Cluster and Fold Stability of E. coli ISC-Type Ferredoxin. PLOS ONE 8: e78948
Pubmed: Author and Title
Google Scholar: Author Only Title Only Author and Title

Yeh C-H, Kaplinsky NJ, Hu C, Charng Y-Y (2012) Some like it hot, some like it warm: phenotyping to explore thermotolerance diversity. Plant Sci Int J Exp Plant Biol 195: 10–23
Pubmed: Author and Title
Google Scholar: Author Only Title Only Author and Title

Yu H, Yang J, Shi Y, Donelson J, Thompson SM, Sprague S, Roshan T, Wang D-L, Liu J, Park S, et al (2017) Arabidopsis Glutaredoxin S17 Contributes to Vegetative Growth, Mineral Accumulation, and Redox Balance during Iron Deficiency. Front Plant Sci 8: 1045
Pubmed: Author and Title
Google Scholar: Author Only Title Only Author and Title

Zaffagnini M, Michelet L, Massot V, Trost P, Lemaire SD (2008) Biochemical characterization of glutaredoxins from Chlamydomonas reinhardtii reveals the unique properties of a chloroplastic CGFS-type glutaredoxin. J Biol Chem 283: 8868–8876
Pubmed: Author and Title
Google Scholar: Author Only Title Only Author and Title

Zhang Y, Liu L, Wu X, An X, Stubbe J, Huang M (2011) Investigation of in vivo diferric tyrosyl radical formation in Saccharomyces cerevisiae Rnr2 protein: requirement of Rnr4 and contribution of Grx3/4 AND Dre2 proteins. J Biol Chem 286: 41499–41509
Pubmed: Author and Title
Google Scholar: Author Only Title Only Author and Title

Zhao C, Wang P, Si T, Hsu C-C, Wang L, Zayed O, Yu Z, Zhu Y, Dong J, Tao WA, et al (2017) MAP kinase cascades regulate the cold response by modulating ICE1 protein stability. Dev Cell 43: 618-629.e5
Pubmed: Author and Title
Google Scholar: Author Only Title Only Author and Title